Chapter 1
Multidimensional NMR: an Introduction

Gareth A. Morris[1] and James W. Emsley[2]

[1]*Department of Chemistry, University of Manchester, Oxford Road, Manchester, M13 9PL, UK*
[2]*School of Chemistry, University of Southampton, Southampton, SO17 1BJ, UK*

1.1	Introduction	3
1.2	Historical Background	4
1.3	Principles and Practicalities	9
1.4	Applications to Liquids	19
1.5	Applications to Liquid Crystals	20
1.6	Concluding Remarks	23
	References	24

1.1 INTRODUCTION

The first demonstration of pulse Fourier transform NMR spectroscopy brought a great improvement in the sensitivity of NMR,[1] and a corresponding widening of its range of applications. Although it was far from obvious at the time, the introduction of FT methods had another, even more profound, consequence for the scope and power of NMR spectroscopy. The change from experiments in which NMR signals were excited and measured simultaneously, as in continuous wave (CW) NMR, to pulsed methods, in which excitation and detection are separated in time, gave the experimenter freedom to manipulate the chemical or physical information content of the data measured, and initiated a florid growth in experimental NMR techniques that has lasted 40 years and shows no sign of abating.

The biggest breakthrough enabled by the separation of excitation and detection in pulsed Fourier transform NMR was the development of multidimensional NMR, in which the idea of a spectrum as a record of signal strength as a function of frequency, $S(F)$, was extended into multiple frequency dimensions, $S(F_1, F_2, \ldots)$. Instead of simply acquiring a free induction decay $s(t)$ following radiofrequency (RF) excitation, free induction decays $s(t_n)$ are acquired using a pulse sequence containing one or more evolution times $t_1, t_2, \ldots t_{n-1}$ for a series of equally spaced values of the evolution times. The complete data matrix $s(t_1, t_2, \ldots t_{n-1}, t_n)$ is then Fourier transformed with respect to $t_1, t_2, \ldots t_{n-1}$, and t_n to yield an n-dimensional spectrum $S(F_1, F_2, \ldots F_{n-1}, F_n)$. (Although the term "multidimensional spectroscopy" in NMR spectroscopy encompasses a wide range of techniques, multidimensional Fourier transform methods dominate, and the term is used here in this sense unless specifically indicated otherwise). By far the commonest family of techniques is two-dimensional, or 2D, NMR spectroscopy, in which free induction decays $s(t_2)$ are acquired for NI increments of an evolution time t_1, and the resultant time-domain data matrix $s(t_1, t_2)$ is Fourier transformed first with respect to t_2 and then with respect to t_1 to give the 2D spectrum $S(F_1, F_2)$. The free induction decays

are sampled every $\Delta t_2 = 1/SW2$ seconds and the evolution time is incremented in steps $\Delta t_1 = 1/SW1$, giving a 2D spectrum with a spectral width of $SW1$ (in hertz) in the F_1 direction and $SW2$ in F_2.

The first advantage of such multidimensional methods is the potential for improved signal resolution. For a normal (or one-dimensional, 1D) spectrum with a spectral width SW, if the frequency range covered by a typical peak is W, then the maximum number of peaks that could, in principle, be resolved is of the order of SW/W. For a 2D spectrum the corresponding number is $SW1 \times SW2/W^2$, which, for typical spectra, represents a large improvement over the 1D case. The second advantage of multidimensional methods is that both the way in which signals are dispersed in a given frequency dimension, and the relationships between those dimensions, depend on the pulse sequence used and are under the direct control of the experimenter. Without this ability to disperse signals differently in different dimensions, there would be no resolution advantage—signals would simply be spread along the diagonal $F_1 = F_2$, with no better resolution than in a 1D spectrum. It is possible to control signal behavior by manipulating the sequence of RF pulses used because even under routine experimental conditions the response of an NMR spin system to RF excitation is nonlinear. NMR is almost unique in this respect, other spectroscopic methods requiring special hardware such as high-powered lasers or microwave amplifiers to drive the spectroscopic response out of the linear regime.

Although the archetypal multidimensional NMR experiments use multiple Fourier transformation of data measured with multiple time domains, neither the Fourier processing nor the measurement of time-sampled data is essential for obtaining the advantages of resolution and enhanced information content. Thus the Fourier transform can be replaced with alternative algorithms (see Chapters 4–10). Such methods are particularly useful where data are sampled nonuniformly in one or more of the time domains, and for high dimensionality ($n>3$) experiments. Similarly, it is also possible to generate multidimensional spectra from data acquired not as a function of evolution time(s), but of experimental variables such as pulsed field gradient strength, as in diffusion-ordered spectroscopy (see Chapter 36), or from time-sampled data where the signal behavior is not oscillatory and hence Fourier processing is inappropriate (see Chapter 37).

1.2 HISTORICAL BACKGROUND

Since the earliest experiments on NMR of liquids, there has been a constant battle to improve spectral resolution. At first, attention was concentrated on minimizing the contribution of static magnetic field inhomogeneity to signal linewidths; it then shifted to increasing the field strength. The introduction of superconducting magnets brought an immediate factor of two improvement in signal separation, but a much larger gain came in 1975 with the first publication of a two-dimensional NMR spectrum.[2] While the use of double-resonance experiments to unravel overlapping multiplets was by that stage commonplace, the idea of using double Fourier transformation of data acquired with two time dimensions had taken a relatively long time to reach fruition. It was first presented formally by Jean Jeener at a conference in Baško Polje, in what is now Croatia, in 1971, but initial experiments were defeated[3] by what is now termed t_1-*noise*.[4] Jeener's experiment consisted simply of two RF pulses separated by a variable evolution time t_1. This pulse sequence is now known as COSY (Correlated SpectroscopY), because it correlates pairs of signals that share a scalar coupling, and over 30 years later it is still one of the most widely used of multidimensional NMR techniques (see Chapters 2, 12 and 13). A paper describing the principles of the new experiment was drafted in November 1971 but never submitted, although the results later appeared in the doctoral thesis of Gerrit Alewaeters ("Een Twee Impulstechniek in Kernmagnetische Resonantie in Vloeistoffen", Vrije Universiteit Brussel, 1976). (The unpublished preprint is notable not just for its clear-sighted analysis of the potential of 2D NMR, but for listing among its advantages "very simple theory"!)

The first successful experiments using a second Fourier transformation were reported in April 1975 by the groups of the future Nobel laureate Richard Ernst,[5] using liquid-state COSY,[2] and of John Waugh,[6] using oscillations in solid-state cross-polarization to resolve heteronuclear dipolar couplings.[7] Later that year, Ernst reported the first liquid-state ^{13}C results, correlating proton-decoupled and proton-coupled ^{13}C spectra,[8] and, in January 1976, the group of Endel Lippmaa reported the use of a second Fourier transformation to record the bandshapes of individual ^{13}C resonances in solids.[9] These early experiments attracted immediate attention, establishing the principle that large gains

in signal resolution could be achieved by dispersing peaks in two independent dimensions F_1 and F_2, using double Fourier transformation of experimental data acquired using a pulse sequence with a variable evolution time t_1. Signal dispersion as a function of F_2 is the same as that in the normal spectrum, but dispersion in the indirect dimension F_1 is determined by the average signal evolution frequency during t_1, giving the experimenter control over the chemical information encoded in the indirect dimension.

In March 1976, the principles of two-dimensional NMR spectroscopy were laid out, and the directions of many future developments defined, in the classic paper of Aue *et al*.[10] This analyzed in detail the effects of the archetypal 2D NMR pulse sequence suggested by Jeener, which consists simply of two RF pulses separated by a variable evolution time t_1, and established a basic structure for a 2D pulse sequence: a preparation period, an evolution period t_1, and a detection period t_2. Amongst other things, this paper analyzed the COSY experiment for AX, AB, and larger spin systems, introduced the terms *cross peak* and *dia (diagonal) peak*, described the use of 2D Fourier methods for magnetic resonance imaging, analyzed the effect of static field inhomogeneity on 2D lineshapes, and illustrated the use of 2D NMR to detect zero- and double-quantum coherences. In a COSY experiment, diagonal peaks appear close to the line $F_1 = F_2$ and arise from signals that remained at the same chemical shift after the second pulse, and cross peaks appear away from the diagonal and arise where scalar coupling causes signals to change chemical shift between t_1 and t_2. A COSY spectrum thus anatomizes the scalar coupling relationships in a proton spectrum, cross peaks appearing wherever a J-coupling is detected between two protons.

At that time spectrometer computers had very limited memory, typically around 16 kilobytes to store both the spectrometer control program and the NMR data acquired, so there was a strong incentive to investigate techniques that, unlike COSY, yield only a narrow range of frequencies in F_1. The next developments were therefore in J-resolved (or 2D J-) spectroscopy (see Chapter 11), in which the evolution period t_1 consists of a modulated spin echo. Here the indirect dimension displays only multiplet structure, and hence requires a much smaller spectral width than the normal spectral dimension F_2. Ernst's group demonstrated a homonuclear J-resolved experiment[11] (giving as a by-product a method for measuring proton spectra without multiplet structure, a prize that had been sought for many years), and that of Freeman developed several variants of heteronuclear 2D J-spectroscopy.[12,13] The latter experiments showed the benefits of suppressing field inhomogeneity contributions to linewidths in the indirect dimension, a gain anticipated in the earlier one-dimensional J-spectroscopy method of Freeman and Hill.[14,15]

It was recognized from the outset that there were problems displaying the results of 2D experiments, because of the nature of the 2D lineshapes, and, as a result, almost all early results displayed the modulus, or absolute value, of the signal rather than its real or imaginary part. The problem of the "phase-twist" lineshape was analyzed by Bodenhausen *et al*.,[16] in a paper that also described and analyzed some of the signal artifacts seen in heteronuclear J-resolved spectra, and by Bachmann *et al*.[17] Both the phase-twist and the artifact analyses were to have lasting impact, the former in the development of methods for phase-sensitive display of 2D spectra with pure absorption mode peaks, and the latter as the stimulus for the development of EXORCYCLE,[18] the first phase cycle to allow the selection of a desired coherence transfer pathway and the prototype for hundreds of subsequent phase cycles.

It was clear from the outset that one of the key applications of 2D NMR would, when instrumentation and software permitted, be to the study of biomolecules. As early as 1977, a homonuclear J-resolved spectrum was reported for a mixture of amino acids,[19] rapidly followed by a J-resolved spectrum of the protein bovine pancreatic trypsin inhibitor.[20,21] This was the beginning of an area of research that was to lead to the award of a second Nobel prize involving multidimensional NMR, to Kurt Wüthrich,[22] and to the establishment of NMR as the method of choice for the determination of 3D structures of proteins and other biopolymers in solution[23] and as one of the primary tools of structural biology.

Up to this point, the highest resolution 2D technique studied was COSY, generating spectra in which signals were dispersed according to the proton chemical shift in both frequency dimensions. The next major step, in 1977, was the extension to heteronuclear 2D correlation (see Chapter 22), in which signals are dispersed as a function of proton chemical shift in one frequency dimension and carbon in the other,[24] offering almost an order of magnitude improvement in resolution because of the combined effects of the wider ^{13}C chemical shift range and the narrower ^{13}C peaks. It was quickly realized[25] that experiments recording

proton free induction decays ("indirect detection") should in principle offer much better sensitivity than those recording ^{13}C signals ("direct detection"). The same paper also made explicit the idea, left implicit in earlier work, of a mixing period between t_1 and t_2. The archetypal structure of a 2D NMR pulse sequence was thus established as consisting of preparation, evolution, mixing (also known as *transfer*—see Chapter 2) and detection periods.

Initially, direct detection methods for heteronuclear chemical shift correlation prevailed, with practical experiments using ^{13}C detection[26] because of the difficulty of achieving adequate suppression of the signals of protons not coupled to ^{13}C. As instrument stability improved, indirect detection methods such as HMQC[27] and HSQC[28] for correlation through one-bond couplings, and HMBC[29] for long-range correlation, took over. The directly detected experiment did however lead, via the loss of its evolution period, to the 1D INEPT pulse sequence, which is now a ubiquitous building block in 2D and 3D pulse sequences for biomolecular structure determination. Indirect detection pulse sequences were also subsequently developed for more specialized purposes, for example, the measurement of long-range heteronuclear coupling constants (see Chapter 23).

As the field of 2D NMR began to consolidate, a number of papers were published that examined the technical underpinning of the method. An analysis of signal-to-noise ratio in 2D techniques[30] showed that the sensitivity penalty on moving from one dimension to two was much smaller than had generally been supposed. Analytical and computational results for the 2D spectra of strongly coupled spin systems[31–34] allowed both direct and iterative analysis of 2D spectra for the extraction of accurate spin system parameters. The application of the projection–cross-section theorem to 2D NMR[35] showed, amongst other things, why it was not possible to obtain an absorption mode decoupled spectrum by 45° projection of a homonuclear J-resolved spectrum; ways around this limitation were only found much later (see Chapter 11).

The steadily increasing number of applications of 2D NMR methods to chemical and biochemical problems brought further stimulus to technical development, for example, the application of heteronuclear correlation methods to the $^{1}H-^{31}P$ spin pair[36] and the investigation of $^{13}C-^{1}H$ dipolar couplings by application of the separated local field (SLF) experiment to a liquid crystalline sample[37] (see Chapter 31). The next big step, however, was the introduction in 1979 of what is now known as the NOESY (*Nuclear Overhauser Effect Spectroscopy*) experiment[38,39] (see Chapter 18), which correlates signals through the exchange of longitudinal magnetization. Although, as the name suggests, it is most often used for the detection of nuclear Overhauser effects, which are caused by through-space dipolar interactions, the same pulse sequence may be used to detect the transfer of magnetization through chemical exchange (where it is sometimes referred to as the *EXSY* (EXchange SpectroscopY) sequence; see Chapter 21. The NOESY experiment and its derivatives were to play a crucial role in the development of NMR as a tool for structural biology,[23,40] allowing, for the first time, the efficient measurement of proton–proton distances in macromolecules. It was also at this stage that the first reviews on 2D methods began to appear.[41,42]

The COSY experiment is very effective at identifying coupling relationships between spins, but ambiguities frequently arise where resonances overlap. Thus the observation of cross peaks at chemical shifts (δ_1, δ_2) and (δ_2, δ_3) could mean that there is a chain of three protons H_1, H_2 and H_3 with couplings J_{H1H2} and J_{H2H3}, or it could simply be that there are two unrelated protons H_{2a} and H_{2b} at the same chemical shift δ_2 with couplings J_{H1H2a} and J_{H2bH3}, and the two spin systems H_1H_{2a} and $H_{2b}H_3$ are completely unrelated. Such ambiguities can be resolved by adding an extra coherence transfer stage to COSY, giving the RELAY (relayed correlation spectroscopy) pulse sequence, which was first described in 1982.[43] At around the same time, the analogous experiment for heteronuclear correlation, in which protons coupled to protons coupled to phosphorus were identified, was also described[44] (see Chapter 15).

The use of 2D NMR to probe multiple-quantum coherences (see Chapters 17 and 32) dates back to Ernst's classic 1976 paper,[10] but chemical applications began in earnest with the extension of the INADEQUATE experiment,[45] in which phase cycling of a pulse pair at the end of a modulated spin echo is used to filter out all ^{13}C signals from molecules with only one ^{13}C spin, to two dimensions.[46] By correlating the signals of directly bonded carbons, this allowed the carbon skeleton of a molecule to be traced out bond by bond, albeit with very low sensitivity. The process of filtering signals through multiple-quantum coherence was applied in more general fashion in multiple-quantum filtered (MQF) COSY.[47] Double-quantum filtration suppresses signals from protons with no couplings, while higher

order filters suppress progressively more and more signals, simplifying spectra.

Filtration experiments such as INADEQUATE and MQF-COSY are designed to improve resolution by *reducing* the number of signals in a 2D spectrum. A further class of homonuclear 2D correlation experiments that complemented COSY and NOESY, and supplanted RELAY, was introduced with the TOCSY (TOtal Correlation SpectroscopY)[48] experiment, also known as HOHAHA (HOmonuclear HArtmann HAhn), in 1983 (see Chapter 16). TOCSY sets out to *increase* the information content of a 2D spectrum by correlating all the spins in a scalar coupling network, using a pulse sequence containing a spin lock period that allows the sequential transfer of magnetization through couplings. Thus while cross peaks arise in COSY where two spins are coupled, and in NOESY where they are close in space or are undergoing mutual chemical exchange, in TOCSY cross peaks can appear for all pairs of protons that are connected by a continuous chain of scalar couplings. TOCSY is thus particularly useful in protein NMR, where each amino acid represents a single isolated network of coupled spins, and different classes of amino acids give different characteristic patterns of TOCSY cross peaks.

Shortly after the introduction of TOCSY, a second class of 2D pulse sequence appeared that also used spin locking, but for a different purpose. The ROESY experiment,[49] as it became known (see Chapter 19), was designed to circumvent the problem that the magnitude of the nuclear Overhauser effect passes through zero as the molecular rotational correlation time approaches the Larmor frequency, dividing the small-molecule regime (rapid motion, positive Overhauser effects) from the large (slow motion, negative Overhauser effects). In ROESY, the spin lock period allows spins to exchange transverse magnetization M_{xy} (as opposed to longitudinal magnetization M_z in NOESY). The effect is to make all species behave as small molecules do in NOESY, giving cross peaks with sign opposite to that of the diagonal peaks, independent of the timescale of molecular motion. Chemical exchange will also give rise to cross peaks, as in NOESY, but this time they are easily distinguished from ROE (rotating-frame Overhauser effect) cross peaks because they have opposite signs. ROESY is significantly more difficult both to perform and to interpret than NOESY, but is useful both for the structural and conformational analysis of intermediate-sized molecules and for studying larger molecules, where spin diffusion can cause problems in NOESY. The practical and interpretational difficulties with ROESY arise because the spin lock period allows other types of coherence transfer as well as the ROE, notably TOCSY-type transfer (see Chapter 20). It is therefore important both to design the spin lock irradiation to maximize discrimination between the ROE and competing transfer mechanisms, and to allow for the existence of the latter effects when analyzing ROESY spectra.

The great majority of 2D spectra produced in the early years used absolute value mode display of the spectral data, to avoid the complications of the phase-twist lineshape and the need to adjust zero and first-order phase corrections in both dimensions, although phase-sensitive mode was sometimes used when plotting cross sections through well-resolved spectra. There are clear disadvantages to using absolute value calculation: its nonlinearity means that signal intensities are distorted where peaks overlap, and severe weighting functions are needed to avoid peak shapes with very wide skirts, degrading both resolution and signal-to-noise ratio. There were therefore strong incentives to devise ways to generate signals with pure absorption mode lineshapes. The first two general solutions to the problem were the hypercomplex method of States *et al.*[50] and the TPPI (time-proportional phase incrementation) method of Marion and Wüthrich[51]; their relative merits have been assessed by Keeler and Neuhaus.[52] Both are still in use, as are hybrids of the two, while absolute value display is still often used for COSY and HMBC experiments. In the case of HMBC, this is because multiplets in F_2 are modulated by scalar couplings, while in COSY, the diagonal and cross peaks are 90° out of phase. (Another reason for favoring absolute value display in COSY experiments is that the antiphase character of the cross-peak multiplet structure can make the time-symmetric weighting functions used to generate acceptable lineshapes a close match to the time-domain signal envelope, approximating matched filtration and giving the absolute value COSY experiment surprisingly good sensitivity.) One major advantage of phase-sensitive homonuclear correlation experiments such as double-quantum filtered (DQF) COSY[53] and exclusive correlation spectroscopy (E.COSY)[54] (see Chapter 14) is that they can allow the accurate measurement of coupling constants.

A third solution to the problem of generating absorption mode 2D lineshapes, which is the commonest in current use, came somewhat later[55] when the availability of actively shielded gradient coils enabled the use of pulsed field gradients to generate complementary echo and antiecho 2D datasets, which can be combined to give pure absorption lineshapes.[56] From the earliest days of 2D NMR, it was appreciated that the key to obtaining clean, informative spectra is to restrict the signals seen to those that have a particular history, or more formally, to suppress all coherences that do not follow the desired coherence transfer pathway[57] during the pulse sequence. Initially, this selection was done exclusively by phase cycling,[58] permuting the phases of RF pulses and of the receiver on successive transients during time averaging, but in recent years, field gradient pulses have been used extensively for coherence transfer pathway selection. Phase cycling is essentially a difference method, canceling out the unwanted signals while retaining the wanted ones, so any instrumental instability will lead to small amounts of the unwanted signals surviving phase cycling. These appear in the 2D spectrum as t_1-noise, streaks of pseudorandom signal along the F_1 direction at the F_2 frequencies of strong signals. One advantage of pulsed field gradients is that they do not rely on subtraction to suppress unwanted signals, so t_1-noise contributions from unwanted pathways are effectively removed. This does not mean, as has sometimes been asserted, that spectra measured using pulsed field gradient methods are free of t_1-noise, but rather that only the wanted signals should contribute to the t_1-noise.

It was clear from the outset that the principle of 2D NMR could be extended to further dimensions, but the practical realization of experiments in three[59] and four[60] dimensions (see Chapter 24) had to wait until computer storage capacities had increased sufficiently to cope with the large quantities of data involved. The primary drive for such extensions came from structural studies on biomolecules, where the extra resolution was critical both for assignment and for the measurement of NOEs. The availability of expression systems for producing proteins with ^{13}C and/or ^{15}N labeling led[61] in the later 1980s to the rapid development of heteronuclear 3D and 4D correlation methods (see Chapters 25, 26, 33 and 34), which can allow the detailed assignment and analysis of the spectra of proteins containing hundreds of amino acids, and to the maturation of multidimensional NMR into one of the two most powerful techniques in modern structural biology (the other being X-ray crystallography).

The explosive growth of 2D NMR and its rapid adoption by chemists meant that the advantages of two-dimensional display of spectral data rapidly became familiar, and were therefore extended to correlation techniques not based on multiple Fourier transformation of time-domain datasets. The most widely used class of experiment in this category is diffusion-ordered spectroscopy or DOSY[62,63] (see Chapter 36), in which Johnson in 1992 took the idea of distinguishing between signals of different species by measuring their rates of diffusion[64] and adapted it for 2D display. In DOSY, pulsed field gradient echo spectra acquired for different gradient amplitudes are analyzed to extract information on the rates of diffusion associated with different signals, and the results presented in 2D or 3D form with signals dispersed according to diffusion coefficient in one dimension. Methods based on numerical approximations to the inverse Laplace transform are also gaining popularity, allowing parameters such as relaxation times and diffusion coefficients to be correlated in multidimensional spectra (see Chapter 37).

There is an important distinction to be drawn between DOSY and other data analysis techniques based on statistical modeling of experimental data, and conventional multidimensional NMR, in which time-domain data are subjected to multiple Fourier transformation. In the latter case, the linearity of the Fourier transform ensures that the frequency-domain spectrum is a faithful representation of the frequencies present in the time-domain data: peaks appear where they belong. In spectra obtained by statistical modeling, the frequencies, diffusion coefficients or other parameters modeled are subject both to statistical uncertainty and to systematic distortion: where peaks end up depends both on the accidents of noise, and on the positions and amplitudes of all the other signals in the spectrum. Thus if two signals in a COSY experiment have the same F_2 frequency and F_1 frequencies of 4.9 and 5.0 ppm, the 2D spectrum will show peaks at $F_1 = 4.9$ ppm and $F_1 = 5.0$ ppm. If two signals in a 2D DOSY experiment have the same F_2 frequency and diffusion coefficients of 4.9 and $5.0 \times 10^{-10}\,m^2\,s^{-1}$, the DOSY spectrum will show a single signal at around $4.95 \times 10^{-10}\,m^2\,s^{-1}$ in the diffusion domain—irrespective of whether monoexponential, biexponential, or more sophisticated fitting is used.

The simplicity, linearity, and familiarity of the Fourier transform have ensured that it remains by far the most general and the most widely used method of obtaining multidimensional spectra; however, a variety of nonlinear processing methods for time-domain data have been developed. They can be highly effective where the behavior of signals is predictable and well understood, using this understanding to impose constraints in the analysis of the experimental data and therefore being able to extract details that the Fourier transform cannot resolve. For example, the F_1 resolution of a 2D spectrum is limited by the number NI of t_1 increments acquired: each increment adds to the overall duration of the experiment, so there is always pressure to truncate sampling in t_1. If the F_1 domain is known to contain only a limited number of individual peaks, even a relatively small NI provides sufficient information to define the frequencies and intensities of those peaks, and a spectrum can be constructed from a much shorter dataset than a 2D Fourier transformation would require to reveal the same level of detail. This is the basis of the 1985 linear prediction[65,66] method (see Chapter 10) and of the 1986 application of maximum entropy reconstruction to phase-sensitive 2D spectra (see Chapter 8). It also underpins the filter diagonalization[67,68] method of 1998 (see Chapter 9).

The beginning of the twenty-first century has seen an explosion of new data-processing methods in multidimensional NMR, mostly driven by the need to avoid the prohibitively long times required by experiments in more than three dimensions. The use of prior knowledge can be taken several stages further in multidimensional NMR. The information content of a multidimensional spectrum can be summarized as the sum of a set of individual peaks, and hence the time-domain data can be modeled as a sum of products of complex exponentials. This principle of multidimensional decomposition was illustrated by the group of Billeter in 2001[69] (see Chapter 6). Because such fitting methods are not constrained to use uniform sampling in all time dimensions, the number of samples needed to achieve clean separation of the limited number of nD peaks is greatly reduced. A completely different approach to a similar goal, introduced in 2003, is to forego Fourier sampling of indirect dimensions and instead to use targeted selective pulses and Hadamard encoding[70] (see Chapter 4). The year 2003 also saw the introduction of the G-matrix Fourier transform or GFT method,[71] which employs synchronous incrementation in parallel time dimensions, using appropriate RF-pulse phase shifts to allow the frequencies with respect to the different dimensions to be separated in sparse spectra, again with a large saving in time.

While the correlation between the behavior of a given signal in different dimensions in a multidimensional NMR experiment is entirely defined by the spin Hamiltonian, it is not necessary to consider the subtleties of spin dynamics to be able to extract useful information from a multidimensional dataset. In many cases, it is sufficient simply to identify related signals by examining the statistics of their evolution, as in covariance spectroscopy,[72] introduced in 2004 (see Chapter 7). Indeed, there is no need for the behaviors correlated to arise from the same spin system or even the same sample; in statistical total correlation spectroscopy (STOCSY),[73] correlations can be identified between signals of different species, or even between different types of spectrum, e.g. NMR and mass spectrometry.

From the outset, the development of multidimensional NMR has gone hand in hand with correspondingly fertile developments in magnetic resonance imaging. The two fields share a common theoretical basis and many instrumental and technical similarities, and in recent years a number of techniques developed in NMR imaging have been successfully applied to spectroscopy. Several methods for reducing the data-acquisition demands of multidimensional spectroscopy have already been mentioned; another, introduced in 2004, adapts the projection–reconstruction method of deriving an image from k-space data[74] to multidimensional spectroscopy[75] (see Chapter 5). Perhaps the most exciting example of such cross-fertilization was Frydman's 2002 adaptation of the concept of very rapid data acquisition by echo-planar imaging[76] to spectroscopy.[77] This uses rapidly switched field gradients to encode data from multiple values of evolution time into a single acquisition, enabling a complete 2D dataset to be acquired from a single excitation (see Chapter 3).

1.3 PRINCIPLES AND PRACTICALITIES

1.3.1 Basics

The formal principles of multidimensional NMR are laid out authoritatively in Chapter 2 and are not

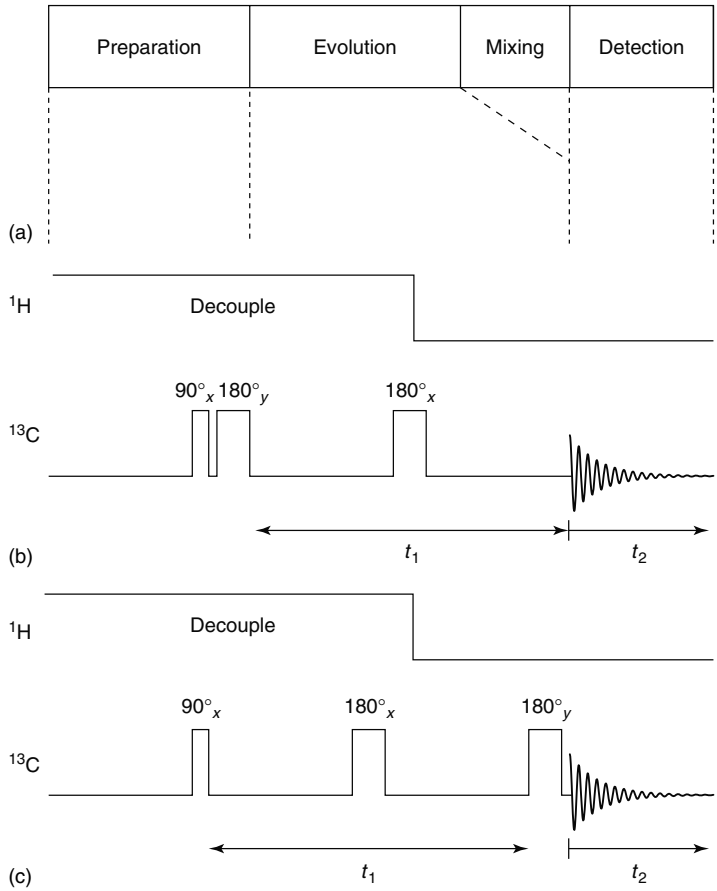

Figure 1.1. (a) Basic structure of a pulse sequence for a two-dimensional NMR experiment. The mixing period is optional. (b) Slightly modified pulse sequence for measuring heteronuclear J-resolved spectra by the "gated decoupler" method. (c) Conjugate sequence to that of (a), in which the apparent sense of precession in t_1 is reversed by the final 180° pulse. Sequences (b) and (c) form an N,R (normal, reversed) pair.

repeated here. The purpose of this section is to explain and to illustrate the practical experimental implications of those principles, initially for classical 2D NMR. Consider a 2D experiment of the archetypal form of Figure 1.1(a). An initial excitation pulse or sequence of pulses at the end of the preparation period will excite coherence between spin states. This may take the form of transverse magnetization (single quantum coherence), or of some other order of coherence, but in either case it will evolve by rotating in spin space through an angle that is proportional to the evolution time t_1, and by decaying at a rate dependent on relaxation and other factors. After the (optional) mixing period, single quantum coherence (transverse magnetization) is measured during the detection period t_2 in the form of a free induction decay $S(t_2)$. As in the evolution period, coherences rotate and decay during the detection period. The net result is that the signal measured may be written as the sum of a set of n components that are phase modulated, typically at different frequencies, as a function of t_1 and of t_2:

$$S(t_1, t_2) = \sum_{j=1}^{n} A_i \mathrm{e}^{2\pi \mathrm{i} F_1{}^j t_1 - \lambda_1{}^j t_1} \mathrm{e}^{2\pi \mathrm{i} F_2{}^j t_2 - \lambda_2{}^j t_2} \tag{1.1}$$

Here it is assumed that the coherence decay is exponential with rate constants λ_1 and λ_2 in t_1 and t_2 respectively; if, as is often ideally the case, coherence

decay is dominated by transverse relaxation, both rate constants will be equal to $1/T_2$. Each component j corresponds to one coherence history, which may involve multiple changes in identity over the course of evolution and mixing, as pulses interchange coherences between pairs of spin states.

Consider as an example the early "gated decoupler" heteronuclear 2D J-spectroscopy experiment with coupled acquisition (see Chapter 11), for which a pulse sequence is shown in Figure 1.1(b). (The particular version of the gated decoupler sequence shown contains a 180° pulse at the start of t_1 that has no effect in an ideal experiment, for reasons that will become clear). For a simple CH group, the F_2 spectrum will be a doublet, the components of which are phase modulated at frequencies $\pm J_{CH}/4$ as a function of t_1. Recording a series of NI free induction decays $s(t_2)$ for equally spaced values of the evolution time t_1 will build up a matrix $s(t_1, t_2)$ of the form shown, in trace and in contour plot form, in Figure 1.2(a). Fourier transformation with respect to t_2 yields a series of NI spectra, $s(t_1, F_2)$, shown in Figure 1.2(b), mapping out the effect of the evolution time on the 1D spectrum. The phases of the two F_2 signals start out the same at $t_1 = 0$, then rotate as a function of t_1, one of them through absorption mode, dispersion, negative absorption, and negative dispersion, and the other, in the opposite sense, through absorption mode, negative dispersion, negative absorption, and positive dispersion. At this point, the computer memory has stored in it a series of F_2 traces for successive values of t_1. The data therefore need to be reordered as t_1 traces, corresponding to a matrix transposition $s(t_1, F_2) \rightarrow s(F_2, t_1)$, to yield Figure 1.2(c), ready for the second Fourier transformation, with respect to t_1, to be performed. This second transformation finally yields the 2D spectrum, the real part of which is shown in Figure 1.2(d). At first sight, Figure 1.2(d) is something of a disappointment: for a spectrum that should contain just two peaks, at $(-J_{CH}/4, \delta_C - J_{CH}/2)$ and $(J_{CH}/4, \delta_C + J_{CH}/2)$, it looks far from simple. The problem, as noted earlier, is that the time-domain signals are phase modulated as a function of t_1, and therefore show the "phase-twist" lineshape in the final 2D spectrum.

The problem of the phase-twist lineshape can be solved in a number of different ways, but before dealing with these, there is another closely related difficulty to consider. As equation (1.1) shows, the basic signal components of multidimensional NMR are phase modulated as a function of both t_1 and t_2. (Clearly, there are many "multidimensional" pulse sequences in which the signal evolution does not follow this pattern, for example where continuous irradiation is used during an evolution period, or where an experimental parameter other than time—for example field gradient amplitude—is incremented, but these are not generally analyzed using multidimensional Fourier transformation or its analogs. Non-FT multidimensional techniques are revisited at the end of this chapter). In many experiments, for example most of those that use a mixing period, signal components come in matched pairs with the same F_2 frequency but equal and opposite F_1 frequencies, so that the time-domain data are phase modulated with respect to t_2 but amplitude modulated with respect to t_1. Thus

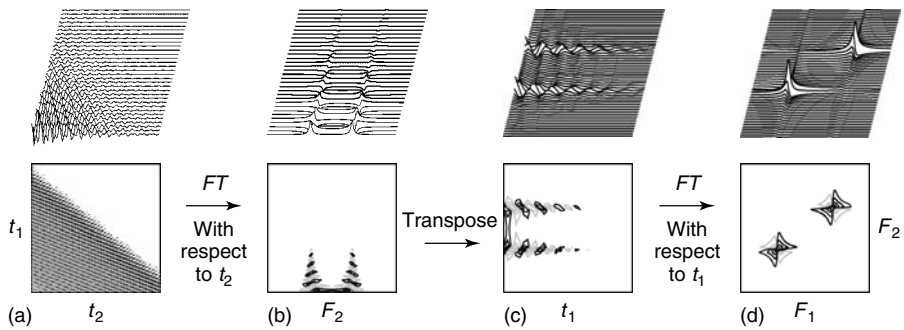

Figure 1.2. Sequence of events in the processing of a synthetic dataset for a CH group subjected to the pulse sequence of Figure 1.1(b), showing (top) stacked trace and (bottom) contour plots of the real part of (a) the raw time-domain data; (b) the data after Fourier transformation with respect to t_2; (c) the result of transposing the latter data matrix; and (d) the final data matrix after Fourier transformation of the transposed data with respect to t_1. Positive contours are drawn in black, negative in gray.

J-resolved spectroscopy, which has no mixing period, is a phase-modulated experiment, whereas COSY and NOESY are amplitude modulated. While 2D Fourier transformation of data phase modulated in t_1 distinguishes directly between positive and negative F_1 frequencies, in amplitude-modulated experiments, intervention is needed to achieve F_1 sign discrimination.

There are four basic methods of restoring F_1 sign discrimination ("F_1 quadrature detection") in amplitude-modulated experiments: phase cycling,[78] time-proportional phase incrementation[51] (TPPI), the so-called States–Haberkorn–Ruben, or hypercomplex, method,[50] and the use of pulsed field gradients,[55,56] as well as various hybrid methods. Which method is used for a given experiment depends, amongst other things, on whether phase-sensitive or absolute value display is required, and on whether pulsed field gradients are available. All four methods rely on changing the relative phase of the coherence in the evolution period and the RF pulses(s) used in the mixing period to determine the sign of F_1. The phase-cycling method uses 90° phase shifts to generate cosine- and sine-modulated datasets, which are added or subtracted during phase cycling to generate a phase-modulated dataset:

$$\begin{aligned} S(t_1, t_2) &= \sum_{j=1}^{n} A_i \cos(2\pi {F_1}^j t_1) \mathrm{e}^{-{\lambda_1}^j t_1} \mathrm{e}^{2\pi \mathrm{i} {F_2}^j t_2 - {\lambda_2}^j t_2} \\ &\quad \pm \mathrm{i} \sum_{j=1}^{n} A_i \sin(2\pi {F_1}^j t_1) \mathrm{e}^{-{\lambda_1}^j t_1} \mathrm{e}^{2\pi \mathrm{i} {F_2}^j t_2 - {\lambda_2}^j t_2} \\ &= 2 \sum_{j=1}^{n} A_i e^{\pm 2\pi \mathrm{i} {F_1}^j t_1 - {\lambda_1}^j t_1} e^{2\pi \mathrm{i} {F_2}^j t_2 - {\lambda_2}^j t_2} \end{aligned} \tag{1.2}$$

Typically a four-step basic phase cycle is used, in which the relative phases of the excitation and mixing RF are changed through 0°, 90°, 180°, and 270°. The first two steps cancel the unwanted components with the wrong sign of F_1 (which give rise to image peaks), and the second two suppress coherences that did not originate in the preparation period (axial peaks). Depending on whether the results of a +90° phase shift are added or subtracted, components with the same sense of modulation in t_1 and t_2 (a "P-type" coherence transfer pathway) or the opposite ("N-type") are selected.

Field gradient pulses are also commonly used for N- and P-type selection. A strong pulse of field gradient will dephase coherences of order greater than zero to the point where they may safely be neglected, but a second pulse of equal effective area will reverse the effect (a "gradient echo"). Since the effect of a gradient pulse depends on the sign of the coherence, a matched pair of gradient pulses of the same sign bracketing the mixing period will select the N-type coherence transfer pathway, and a pair of pulses of opposite sign will select the P-type.

N- or P-type selection, whether by phase cycling or by pulsed field gradients, gives a phase-modulated dataset. This will transform to a 2D spectrum in which peaks appear at the correct positions (F_1, F_2), but those peaks have the so-called "phase-twist" lineshape. This lineshape originates from the familiar absorption and dispersion modes seen in one-dimensional NMR. For the free induction decay of a single resonance of unit amplitude, decay constant λ, and frequency F^0, the real part of the Fourier transform is the absorption mode spectrum $A(F^0, \lambda; F)$ and the imaginary part the dispersion mode $D(F^0, \lambda; F)$:

$$\begin{aligned} FT^- \left(\mathrm{e}^{-\mathrm{i}2\pi F^0 t - \lambda t}\right) &= \int_0^\infty \mathrm{e}^{-\mathrm{i}2\pi F t} e^{\mathrm{i}2\pi F^0 t - \lambda t} \mathrm{d}t \\ &= \frac{\lambda}{4\pi^2 \left(F - F^0\right)^2 + \lambda^2} \\ &\quad + \frac{\mathrm{i}2\pi\lambda \left(F - F^0\right)}{4\pi^2 \left(F - F^0\right)^2 + \lambda^2} \\ &= A\left(F^0, \lambda; F\right) + \mathrm{i}D\left(F^0, \lambda; F\right) \end{aligned} \tag{1.3}$$

The absorption mode has a purely positive-going lineshape with a width at half height of λ/π Hz; the dispersion mode is much wider, and is antisymmetric about F^0. In a 2D NMR experiment, double Fourier transformation of a unit intensity phase-modulated component of the form of equation (1.1) thus yields

$$\begin{aligned} &FT_{t_1}^- \left[FT_{t_2}^- \left(\mathrm{e}^{2\pi \mathrm{i} F_1^0 t_1 - \lambda_1 t_1} \mathrm{e}^{2\pi \mathrm{i} F_2^0 t_2 - \lambda_2 t_2} \right) \right] \\ &\quad = FT_{t_1}^- \left(\mathrm{e}^{2\pi \mathrm{i} F_1^0 t_1 - \lambda_1 t_1} \right) \times FT_{t_2}^- \left(\mathrm{e}^{2\pi \mathrm{i} F_2^0 t_2 - \lambda_2 t_2} \right) \\ &\quad = \left[A\left(F_1^0, \lambda_1; F_1\right) + \mathrm{i}D\left(F_1^0, \lambda_1; F_1\right) \right] \\ &\qquad \times \left[A\left(F_2^0, \lambda_2; F_2\right) + \mathrm{i}D\left(F_2^0, \lambda_2; F_2\right) \right] \\ &\quad = \left[A\left(F_1^0, \lambda_1; F_1\right) A\left(F_2^0, \lambda_2; F_2\right) \right. \\ &\qquad \left. - D\left(F_1^0, \lambda_1; F_1\right) D\left(F_2^0, \lambda_2; F_2\right) \right] \\ &\qquad + \mathrm{i} \left[A\left(F_1^0, \lambda_1; F_1\right) D\left(F_2^0, \lambda_2; F_2\right) \right. \\ &\qquad \left. + D\left(F_1^0, \lambda_1; F_1\right) A\left(F_2^0, \lambda_2; F_2\right) \right] \end{aligned} \tag{1.4}$$

The real part of the 2D lineshape consists of two terms, inextricably mixed: a purely positive double

absorption mode, and a broad double dispersion mode with two positive and two negative lobes. The net result is a lineshape in which a cross-section taken through F_2 at increasing F_1 changes from positive dispersion at $F_1 \ll {F_1}^0$ to absorption at $F_1 = {F_1}^0$ to negative dispersion at $F_1 \gg {F_1}^0$—the notorious "phase twist".

One solution to the problems posed by the phase-twist lineshape is to use aggressive time-domain weighting to force the time-domain signals into a symmetric envelope, then use absolute value (also known as *modulus* or *magnitude*) display. This gives a broader but approximately absorption mode shape to isolated peaks, but is costly in signal-to-noise ratio and resolution, and leads to distorted intensities where peaks overlap. There is therefore a powerful incentive to tame the phase-twist lineshape by canceling its double dispersion component. One key difference between the absorption and dispersion modes is their symmetry: the absorption mode is symmetric, the dispersion antisymmetric. The double dispersion component can therefore be canceled by adding together a 2D spectrum and the F_1 mirror image of the same spectrum measured with the opposite sign of modulation as a function of t_1. This is particularly simple where F_1 quadrature detection is achieved with field gradient pulses, since a change in sign of one gradient pulse changes the data from N-type to P-type modulation. The operation of taking the mirror image of the Fourier transform of a function is equivalent to Fourier transforming the complex conjugate of that function. Thus the production of a double absorption mode 2D spectrum using N,P pathway selection reduces to acquiring the two datasets, Fourier transforming both with respect to t_2, changing the sign of the imaginary component of one of the two datasets, adding them together, and Fourier transforming with respect to t_1:

$$\begin{aligned} S(F_1, F_2) &= FT_{t_1}^{-}\left[FT_{t_2}^{-}\left(\mathrm{e}^{2\pi\mathrm{i}F_1^0 t_1-\lambda_1 t_1}\mathrm{e}^{2e\mathrm{i}F_2^0 t_2-\lambda_2 t_2}\right)\right. \\ &\quad \left. + \left\{FT_{t_2}^{-}\left(\mathrm{e}^{-2\pi\mathrm{i}F_1^0 t_1-\lambda_1 t_1}\mathrm{e}^{2\pi\mathrm{i}F_2^0 t_2-\lambda_2 t_2}\right)\right\}^{*}\right] \\ &= FT_{t_1}^{-}\begin{bmatrix} \mathrm{e}^{2\pi\mathrm{i}F_1^0 t_1-\lambda_1 t_1}\left\{A\left(F_2^0, \lambda_2; F_2\right)\right. \\ \left. \quad +\mathrm{i}D\left(F_2^0, \lambda_2; F_2\right)\right\} \\ +\mathrm{e}^{2\pi\mathrm{i}F_1^0 t_1-\lambda_1 t_1}\left\{A\left(F_2^0, \lambda_2; F_2\right)\right. \\ \left. \quad -\mathrm{i}D\left(F_2^0, \lambda_2; F_2\right)\right\} \end{bmatrix} \\ &= 2A\left(F_1^0, \lambda_1; F_1\right) A\left(F_2^0, \lambda_2; F_2\right) \\ &\quad + 2\mathrm{i}D\left(F_1^0, \lambda_1; F_1\right) A\left(F_2^0, \lambda_2; F_2\right) \end{aligned} \tag{1.5}$$

The real part of the result then shows the desired double absorption mode lineshape, while the imaginary part shows absorption in F_2 and dispersion in F_1. The above assumes that all signals are correctly phased in the original experimental data; in practice, phases are adjusted after the double Fourier transformation by retaining both the sum and the difference terms and taking a suitable linear combination. Phasing in two dimensions thus requires taking a linear combination of four different components (here the real and imaginary results for sum and for difference processing), with coefficients determined by four phase parameters, the zero and first-order phase correction parameters for the two frequency dimensions F_1 and F_2.

The States–Haberkorn–Ruben and the TPPI method are both designed to generate double absorption peaks from amplitude-modulated data. The States method uses two different experimental phase cycles to generate a cosine-modulated and a sine-modulated dataset, and Fourier transforms them with respect to t_2. It then combines the absorption mode of the cosine dataset with i times that of the sine dataset, and Fourier transforms the result to give a spectrum whose real part has double absorption lineshapes:

$$\begin{aligned} S(F_1, F_2) &= FT_{t_1}^{-}\begin{bmatrix} \mathrm{Re}\left\langle FT_{t_2}^{-}\left\{\cos\left(2\pi\mathrm{i}F_1^0 t_1\right)\right.\right. \\ \left.\left. \quad \times \mathrm{e}^{-\lambda_1 t_1}\mathrm{e}^{2\pi\mathrm{i}F_2^0 t_2-\lambda_2 t_2}\right\}\right\rangle \\ \quad +\mathrm{i}\ \mathrm{Re}\left\langle FT_{t_2}^{-}\left\{\sin\left(2\pi\mathrm{i}F_1^0 t_1\right)\right.\right. \\ \left.\left. \quad \times \mathrm{e}^{-\lambda_1 t_1}\mathrm{e}^{2\pi\mathrm{i}F_2^0 t_2-\lambda_2 t_2}\right\}\right\rangle \end{bmatrix} \\ &= FT_{t_1}^{-}\left[\mathrm{e}^{2\pi\mathrm{i}F_1^0 t_1-\lambda_1 t_1} A\left(F_2^0, \lambda_2; F_2\right)\right] \\ &= A\left(F_1^0, \lambda_1; F_1\right) A\left(F_2^0, \lambda_2; F_2\right) \\ &\quad + \mathrm{i}D\left(F_1^0, \lambda_1; F_1\right) A\left(F_2^0, \lambda_2; F_2\right) \end{aligned} \tag{1.6}$$

Again, in practice phases are adjusted after the double Fourier transformation by retaining both the real and the imaginary parts of the two datasets after the first Fourier transformation. Since there are two orthogonal relationships, between the real and imaginary parts of the data after the first transformation and between those after the second, the data treatment can be regarded as using two distinct

imaginary domains, hence the alternative name of the hypercomplex method.

In the TPPI method, both the timing and the phases of the basic pulse sequence are changed. TPPI solves the problem of discriminating between F_1 signals of different signs by shifting all F_1 frequencies by half the F_1 width $SW1$ of the spectrum, so that instead of running from $-(SW1)/2$ to $+(SW1)/2$ Hz the experimental data are measured with respect to a frequency $F_1' = F_1 + (SW1)/2$. To avoid folding, this requires that the spectral width in F_1' be twice that in F_1, so the first change is that t_1 is now incremented in steps of $1/(2\,SW1)$ instead of $1/SW1$ in the TPPI method. The reason for the second change is that to effect the shift in frequency, the relative phases of the excitation and mixing stages are incremented by 90° each time the evolution period is incremented. The result is a dataset, which, if Fourier transformed normally, would show all signals with phase-twist lineshapes and with mirror symmetry in F_1'. However, since it is no longer necessary to know the sign of F_1', no information is needed about signal phase as a function of t_1, and the imaginary (dispersion mode) part of the data after the first Fourier transform can be discarded:

$$\begin{aligned}
&S(F_1', F_2)\\
&\quad = FT_{t_1}^{-}\left[\mathrm{Re}\left\langle FT_{t_2}^{-}\left\{\cos\left(2\pi\left(F_1^0 + \frac{(SW1)}{2}\right)t_1\right)\right.\right.\right.\\
&\qquad \left.\left.\left.\times\ \mathrm{e}^{-\lambda_1 t_1}\mathrm{e}^{2\pi \mathrm{i} F_2^0 t_2 - \lambda_2 t_2}\right\}\right\rangle\right]\\
&\quad = FT_{t_1}^{-}\left[\cos\left(2\pi\left(F_1^0 + \frac{(SW1)}{2}\right)t_1\right)\right.\\
&\qquad \left.\times\ \mathrm{e}^{-\lambda_1 t_1} A(F_2^0, \lambda_2; F_2)\right]\\
&\quad = A\left(F_1^0 + \frac{(SW1)}{2}, \lambda_1; F_1'\right) A(F_2^0, \lambda_2; F_2)\\
&\qquad + \mathrm{i}D\left(F_1^0 + \frac{(SW1)}{2}, \lambda_1; F_1'\right) A(F_2^0, \lambda_2; F_2)\\
&\qquad + A\left(-F_1^0 - \frac{(SW1)}{2}, \lambda_1; F_1'\right) A(F_2^0, \lambda_2; F_2)\\
&\qquad + \mathrm{i}D\left(-F_1^0 - \frac{(SW1)}{2}, \lambda_1; F_1'\right) A(F_2^0, \lambda_2; F_2)
\end{aligned} \tag{1.7}$$

Here the desired double absorption spectrum and its mirror image appear side-by-side in F_1'. Half of the F_1' domain is discarded, leaving the required spectrum running from 0 to $SW1$ in F_1', i.e., from $-(SW1)/2$ to $+(SW1)/2$ in F_1. In practical implementations, either the mirror image is discarded automatically, or a real FT is used, and as previously the F_2 imaginary component is retained to allow phases to be adjusted after the second Fourier transformation.

The phase-sensitive methods described above also point the way to obtaining pure absorption lineshapes in some (but not all) of the minority of experiments that show phase modulation as a function of F_1. The double dispersion contribution to the phase-twist lineshape can be canceled by combining datasets in which either the true, or the apparent, sense of the phase modulation with respect to t_1 is reversed. The former method is only possible in a few cases; one example is that of J-resolved spectroscopy by the gated decoupler method (see Chapter 11), where reversing the order of the two halves of the evolution period can have the desired effect[78] (but only where decoupling is applied in t_2[79]). The latter method requires a 180° rotation to be applied to the relevant coherences at the end of the evolution period, but is only applicable where that rotation can be applied without generating unwanted mixing, for example, in decoupled heteronuclear J-resolved spectroscopy[17] or in the Pell–Keeler method for homonuclear J-resolved spectroscopy.[80] By analogy with phase-sensitive 2D NMR methods that use N,P pathway selection, the parent sequence and the variant with a 180° pulse at the end of t_1 may be termed an N,R pair, with N standing for normal and R for reversed t_1 modulation.

Returning to the gated decoupler experiment of Figure 1.1(b), repeating the experiment with the pulse sequence of Figure 1.1(c) will give a 2D spectrum of the form shown in Figure 1.3(a), with the signs of the F_1 frequencies of the two peaks (but not those of the phase-twist lineshapes) reversed compared to Figure 1.2(d). (The reason for the extra 180°_y pulse in Figure 1.1(b) is to ensure that the sequences of Figure 1.1(b) and (c) generate equal signal amplitudes even where imperfect instrumentation is used; this is a common feature of N,R-type experiments). Reflecting the spectrum of Figure 1.3(a) about the axis $F_1 = 0$ gives Figure 1.3(b), in which the peak positions are the same as those in Figure 1.2(d), reproduced as Figure 1.3(c), but the signs of the double dispersion component of the phase-twist lineshape are opposite. Adding the data of Figure 1.3(b) (c) then finally gives the desired outcome of a 2D spectrum in which all signals have a pure double absorption lineshape.

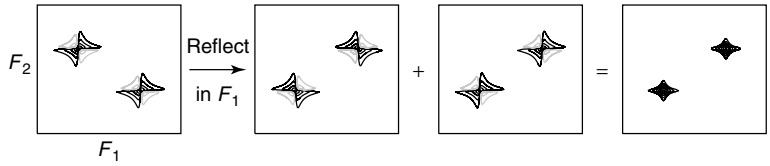

Figure 1.3. Frequency-domain illustration of the production of a pure absorption mode 2D J-resolved spectrum using data acquired using the pulse sequences of Figure 1.1(b) and (c). The 2D spectrum (a) produced by applying the processing steps of Figure 1.2 to data calculated for the sequence of Figure 1.1(c) is reflected about the axis $F_1 = 0$. This gives a reversed spectrum (b) in which the peak positions are the same as those in Figure 1.2(d) but the sense of rotation of the phase-twist lineshape is reversed. Adding this to the latter spectrum (c) yields a pure absorption mode 2D spectrum (d) in which the double dispersion mode contributions to the phase-twist lineshape in (b) and (c) have canceled each other out.

1.3.2 Higher Dimensions

So far, the discussion has been confined to 2D NMR, but clearly the same principles and methods extend to higher dimensionalities. As the number of dimensions n increases, so do both the volume of data involved, and the time needed to acquire those data. Because the number of different combinations of real and imaginary outputs of successive Fourier transformations increases as 2^n, it is helpful to preset the phase adjustment before processing (see Chapter 25) rather than retain all 2^n components. With appropriate evolution period timing and careful control of off-resonance effects it is often possible to arrange that no phase correction is needed in indirect dimensions. There is also a strong incentive to make do with the minimum possible number of experimental data points in the indirect dimensions, as well as to minimize the time between measurements.

The high cost in experimental time of digitizing the indirect dimensions where $n > 2$ makes the choice of data-processing method in these dimensions very important. Simple Fourier transformation, as commonly used in 2D NMR, requires careful choice of weighting function (typically Gaussian) to minimize truncation artifacts ("sinc wiggles") and is inherently limited in the resolution achievable. Most of the higher dimensionality experiments are designed for use with labeled proteins, limiting both the range of different signal intensities expected and the number of different signals. There is, therefore, considerable scope for using prior knowledge to constrain the data analysis and thereby enhance the precision of the results. The price paid is that there is no longer a linear relationship between time- and frequency-domain data, and hence there is more chance of the processing generating misleading results. Thus linear prediction (see Chapter 10), which extrapolates measured data on the assumption that they can be satisfactorily modeled by the sum of a finite number of rotating and decaying exponentials, followed by Fourier transformation, is a very effective and relatively safe way to improve resolution by a factor of 2 or more in indirect dimensions. The filter diagonalization method (see Chapter 9) can retrieve good resolution from much shorter time series, at the expense of an increased risk of misrepresenting spectral features.

Once the principle of nonlinear data processing has been accepted, the experimenter is no longer tied to the discipline of acquiring data at regular intervals in each of the indirect dimensions. All that is necessary is that the sampling in these dimensions be sufficiently representative for all the expected spectral features to be distinguishable. The limit of such an approach is where it is known beforehand that there is only a single exponentially decaying signal present, with a frequency between $+F_{\max}$ and $F_{\max}$. Here just two measurements are needed, a time $\leqslant 1/(2F_{\max})$ apart, to determine the frequency and the linewidth of the signal, from the phase difference and the relative amplitude of the two measured data points, respectively.[81,82]

The principle of sparse sampling is a powerful one, and indeed offers the only practical route to very high dimensionality ($n > 4$) spectra. Many different strategies have been tried, which differ in the nature of the assumptions made about signal behavior in the indirect dimensions and in their susceptibility to error. Sampling just two data points is an extreme case, requiring the assumption of a single signal in the relevant dimension. At the other extreme, maximum entropy methods (see Chapter 8) can be used with a wide variety of sampling strategies and assume only that a reconstruction with minimum information content will suffice. Where signals are

relatively sparse, projection–reconstruction methods (see Chapter 5) use sampling at equal intervals along restricted directions in the indirect dimensions, and can be very effective; this approach shares with maximum entropy reconstruction a lack of restrictive assumptions but a susceptibility to small artifacts that limits its use in spectra with high dynamic range. An alternative approach to sparse spectra is to model multidimensional experimental data in the time domain as the sum of a finite set of contributions, each of which is the product of one function $F(t)$ for each time domain (see Chapter 6); here, as with maximum entropy reconstruction, there are few constraints on the sampling pattern chosen.

In many cases, the information available to the spectroscopist goes well beyond simple assumptions about sparseness or simplicity. In homonuclear correlation experiments, for example, the only frequencies that can appear in an indirect dimension are those that exist in the directly observed dimension. Given this information, it is possible to take a time-domain dataset containing $N_1 \times N_2$ data points and reconstruct a 2D frequency spectrum with a resolution of $N_2 \times N_2$ points by examining the covariance of signals at different F_2 frequencies as a function of t_1 (see Chapter 7). This approach can be extended to the coprocessing of two 2D heteronuclear correlation spectra sharing only one common nucleus to produce a 2D correlation spectrum for the other two, for example, constructing a $^{13}C-^{15}N$ correlation spectrum from a ^{15}N HSQC and a ^{13}C HMBC spectrum (provided that the ^{1}H spectrum is nondegenerate). Prior knowledge of the form of the directly observed spectrum can also be used in a very direct way in sparse spectra, by restricting excitation solely to those frequencies at which signals appear, and multiplexing data acquisition using Hadamard encoding (see Chapter 4); again, great savings in experiment time can be obtained in multidimensional experiments.

So far, all the methods described have treated the sample as monolithic, but of course it is distributed over the active volume of the detector coil. It is therefore possible to probe different parts of the spectrum, or different regions of indirect domains, at different positions in the sample. An early example of such an approach was the pure shift proton spectroscopy method of Zangger and Sterk[83] (see Chapter 11). A much more general approach, based on echo-planar imaging techniques, is to use each horizontal slice of the sample for a different value of an evolution time (see Chapter 3). This allows a full 2D dataset to be acquired in a single scan, albeit with limited resolution in the indirect dimension. Such methods allow time-resolved 2D spectra to be measured with a resolution of the order of seconds. This is by no means the only route to rapid measurement of 2D spectra; a very simple approach that is also effective (see Chapter 35) is to minimize the perturbation of the spins being measured by using selective pulses and/or reduced flip angle excitation, thus allowing much shorter recycle times to be used.

1.3.3 Practical Problems

Conventional one-dimensional spectra are composed almost exclusively of signals, which are wanted, and a background of noise, which is not. Multidimensional spectra, however, have a more varied composition. Because RF pulses are necessarily imperfect, having finite duration (allowing off-resonance effects), and less than perfect spatial homogeneity (meaning that different parts of the sample experience different spin rotations), signals can follow a range of different coherence transfer pathways, and hence acquire a range of different frequencies in indirect dimensions. Although considerable effort goes into designing phase cycles and sequences of field gradient pulses to suppress signals from unwanted pathways, where the basic signal-to-noise ratio is good it is usual to see artifact peaks from the rejected pathways. Pulsed field gradients are generally more effective at suppression than phase cycling, but even these are limited because of the need to avoid undesirable effects such as field (and hence lineshape) disturbance, diffusional attenuation, J-modulation and so on. In interpreting multidimensional spectra with high dynamic range, it is therefore important to be aware of the likely positions of artifact peaks (e.g., as F_1 mirror images of strong peaks).

A second class of artifacts arises because of the need to keep experiment time to a minimum. The trade-off between time and signal-to-noise ratio is familiar in one-dimensional NMR, where the worst that can happen if pulsing is too rapid is that peaks may show phase and intensity anomalies.[84] In multidimensional NMR, there is a more serious problem with leaving insufficient recovery time between transients, which is that the deviations from equilibrium at the end of one transient may survive into the next. Since these deviations, which may take the form of nonequilibrium spin state populations or

of coherences, are generally modulated as a function of the evolution period in the first transient, the effect of a second application of the pulse sequence is to generate extra, spurious, t_1 modulations. As a result, signals appear with unexpected F_1 frequencies; a common symptom of too-rapid pulsing in homonuclear correlation experiments is the presence of multiple diagonal peaks (often folded in F_1) with $F_1 = F_2 \pm nF_2$, where n is an integer. Careful choice of phase cycle can reduce but not eliminate such artifacts;[85] pulsed field gradients are generally more effective, partly because the unwanted signals are then attenuated by diffusion.

In concentrated samples, there is a third, more exotic, source of spurious signals, in the perturbation of spin dynamics by the magnetic fields that those spins produce.[86,87] There are typically two mechanisms involved: the direct effect of the dipolar magnetic field generated by the spins (confusingly known as the *dipolar demagnetizing field*), and the rotating magnetic field, usually much stronger, generated by the currents induced in the receiver coil by precessing transverse magnetizations (known as the *radiation damping* field). The latter mechanism is particularly prevalent with low temperature probes (cryoprobes) because of their high quality factors Q. Both mechanisms lead to multiple spurious F_1 responses, typically at harmonics, sums, and differences of the expected frequencies. Dipolar demagnetizing field effects can be minimized by the use of field gradients oriented at the magic angle to the static field B_0, but radiation damping effects are less tractable.

So far all of the artifacts considered have been coherent in t_1, resulting in individual peaks in F_1. There is a further class of artifact that often appears as apparently random streaks of signals across F_1, "t_1-noise", at the F_2 frequencies of strong signals. In multidimensional NMR, information on the indirect dimensions (e.g., F_1 in 2D NMR) is obtained by mapping out modulations as a function of evolution time in a point-by-point manner, with measurements generally some seconds apart. Any instrumental irreproducibility on this timescale, for example, a change in pulse phase or flip angle, will cause the actual signal measured to differ from the expected value. If the errors in successive measurements are uncorrelated, the effect will be that a small proportion of the true signal ends up spread randomly across the whole range of possible F_1 values, giving the characteristic noisy streaks of t_1-noise. Such problems are particularly acute if phase cycling is used to separate out a weak signal from among stronger signals that follow unwanted coherence transfer pathways, since the level of the t_1-noise is determined by the strong unwanted signals rather than the weak wanted one.

Perturbations that affect the amplitudes, phases, frequencies, and lineshapes of signals can all give rise to t_1-noise. Many such perturbations are coherent in origin, for example, lack of spectral purity (both receiver and transmitter waveforms typically have low-level modulations at the AC power supply frequency, 60 Hz in the Americas, 50 Hz in most other places), but give rise to apparently incoherent effects. More troublesome are very slow coherent modulations, since the modulations in real time map directly onto the sequential measurement of signal as a function of evolution time, and hence give rise to coherent modulation sidebands in F_1. A common example is the appearance of "air-conditioning sidebands" in F_1, caused by oscillations in room temperature driven by air-conditioning equipment. A very effective strategy for minimizing the impact of room temperature oscillations (and of some rapid-pulsing artifacts) is to acquire the individual free induction decays for different values of evolution time in random order.[88]

Figure 1.4 illustrates the impact of some of these sources of artifacts on a simple COSY spectrum, measured with routine parameters on a relatively old, and hence rather unstable, 300 MHz spectrometer. Pulsed field gradients were not used, F_1 quadrature detection relying on phase cycling, and the second pulse of the COSY sequence was reduced in flip angle to 30° to allow the relative signs of coupling constants to be determined for the acyl nitroso Diels–Alder adduct shown.[89] The most obvious problem is the three streaks of t_1-noise seen for the signals appearing at 2.9, 6.6, and 6.8 ppm (these signals are actually folded from outside the spectral width, but that does not affect the result here). The t_1-noise is proportionately worse for the signal at 6.8 ppm, with a signal-to-t_1-noise ratio of about 300 : 1, than for that at 2.9 ppm (600 : 1), as lock instability has more effect on narrow signals than on broad ones. Signal-to-t_1-noise ratios on modern spectrometers can be much better than these, approaching 10 000 : 1 in favorable circumstances; a further order of magnitude improvement can be obtained by reference deconvolution. The recycle time of 5 s used here is sufficient to avoid rapid-pulsing artifacts for the signals of interest, between 4 and 6 ppm, but axial peaks (along the arrowed line) are seen for the strong signals and

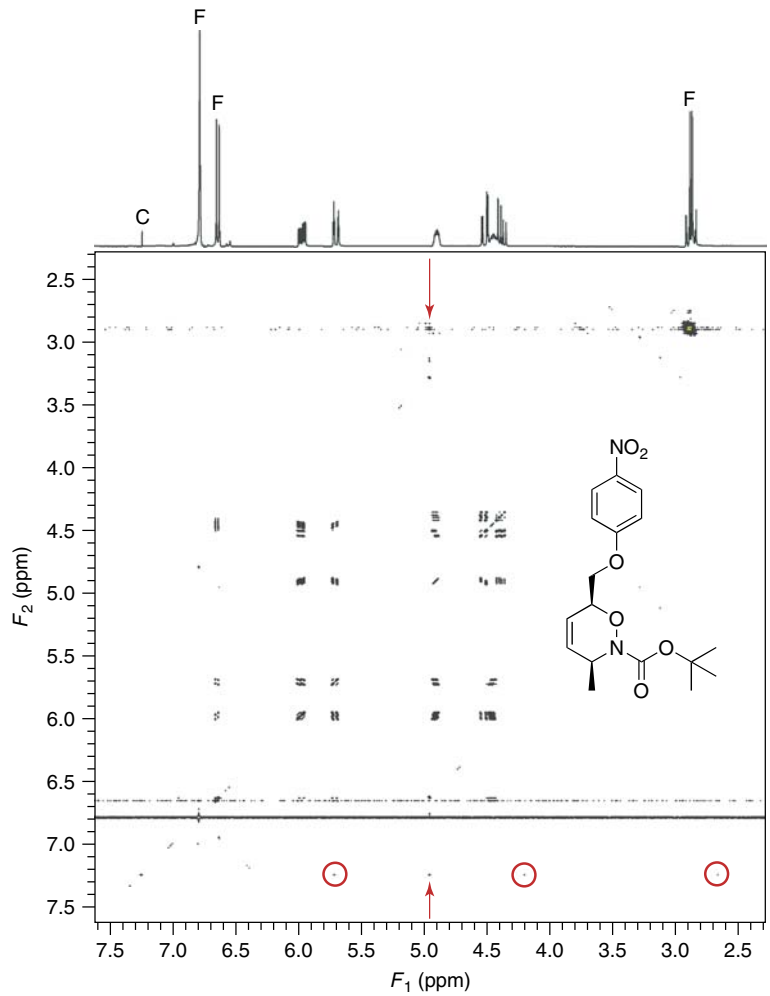

Figure 1.4. Proton COSY spectrum measured at 300 MHz for a $CDCl_3$ solution of the acyl nitroso Diels–Alder adduct shown in the inset, using a phase cycled pulse sequence without pulsed field gradients and with the flip angle of the second pulse reduced to 30°. Four transients were acquired for a total of 2048 increments with a recycle time of 5 s; sine bell weighting was used in both dimensions. Peaks marked F were folded from outside the spectral width to improve digitization. Axial peaks lie along the line $F_1 = 0$, corresponding to a chemical shift of 4.95 ppm, marked by the vertical arrows, and additional rapid-pulsing artifacts for the residual protio-chloroform peak C are marked by circles. (Sample kindly provided by Dr. A.V. Stachulski.)

for some impurities with long spin–lattice relaxation times. The residual protiochloroform peak C at $\delta_C = 7.24$ ppm shows strong rapid-pulsing artifacts because of its long T_1; in addition to the arrowed axial peak, circled rapid-pulsing artifacts are seen at the frequencies of $-\delta_C$, $2\delta_C - SW1$, and $-(2\delta_C - SW1)$, the latter two having been folded in F_1. While t_1-noise and rapid-pulsing artifacts are often much less obvious in published spectra of low dynamic range, particularly when nonlinear data manipulations such as symmetrization have been used, it is rare for them not to be visible on examination of the original data, and care should always be taken in the interpretation (whether automated or manual) of multidimensional NMR data, to avoid being misled by artifacts.

1.4 APPLICATIONS TO LIQUIDS

Multidimensional NMR has been responsible for major changes in the ways in which NMR spectroscopy is applied in a number of fields. In chemical structure elucidation, it has led to a shift from precedent-based methods, relying largely on skilled interpretation of the values of the chemical shifts and coupling constants measured, towards evidence-based methods, in which correlations through bonds and through space are used to map out structures.[90] Evidence-based methods reach their current apogee in structural biology, where fully automated spectral analysis is growing in importance, and in areas such as NMR crystallography.[91] In small-molecule NMR, automated methods have been developed and continue to show promise, but have yet to make a significant impact. This is in part because the structural variety of organic chemistry makes the enumeration of the structural possibilities consistent with given NMR data a much greater technical challenge than is the case for peptides or oligonucleotides, and in part because the great reservoir of interpretational experience shared by synthetic chemists and NMR spectroscopists makes a formidable competitor.

The historical growth of *n*D NMR methods was, in its early years, dominated by the development of techniques for the structure elucidation of small molecules in solution. The classical techniques of homo- and heteronuclear 2D correlation, such as COSY, NOESY, ROESY, TOCSY, HMQC/HSQC, and HMBC, and to a lesser extent, INADEQUATE, now form both a routine background to most research in synthetic chemistry, and a standard part of an education in chemistry. Such methods are now so familiar in organic chemistry that it is easy to forget that the periodic table offers a wealth of magnetic nuclei beyond the proton and ^{13}C; there are many applications for multidimensional experiments involving other nuclei (see, for example, Chapters 27 and 28).

While small-molecule techniques drove their initial development, part of the blossoming of multidimensional NMR methods arose from the happy accident that parallel developments in molecular biology allowed the ready production of biomolecules, particularly proteins, incorporating ^{13}C, ^{15}N, and, more recently, ^{2}H, labels. This had three important consequences. First, the much greater dispersion of chemical shifts for ^{13}C and ^{15}N compared to ^{1}H allowed the routine resolution of the signals of individual spins even in large (tens of kilodaltons) molecules. Second, the presence of multiple magnetic isotopes provided an incentive for the development of 3D and 4D NMR methods, allowing, for example, proton signals and proton–proton correlations, respectively, to be resolved for a specific combination of ^{13}C and ^{15}N chemical shifts. Third, the presence of directly bonded magnetic nuclei throughout the skeleton of a biomolecule gave a very direct route to the assignment of resonances.

Early work on protein structure determination by NMR rapidly established a basic paradigm (see Chapter 33). In outline, through-bond experiments such as COSY and TOCSY are used to assign coupled proton spin systems to different classes of amino acids, based on characteristic patterns of connectivity and chemical shifts. Through-space NOESY data are then used to assign each spin system to a specific amino acid in the primary sequence, for example, by tracing out the alternate through-bond coupling relationships between NH and α-CH in a single residue and through-space relationships between α-CH on one residue and NH on the next, and by identifying secondary structure elements such as α-helices and β-sheets. Finally, the intensities of the cross peaks in the full NOESY dataset are used to triangulate the positions of the individual protons and refine the three-dimensional protein structure, typically using distance geometry and/or molecular dynamics algorithms.

The critical need for improved resolving power provided the initial stimulus for the extension from 2D methods to 3D, with experiments such as COSY-NOESY and NOESY-TOCSY (see Chapter 24). The introduction of ^{13}C and ^{15}N enrichment led rapidly to the development of 3D and 4D methods to exploit the extra resolution afforded by ^{13}C and ^{15}N chemical shifts, applied first to resolving NOESY planes as a function of ^{13}C or ^{15}N chemical shift (see Chapter 25), and, subsequently, to a very wide range of experiments tailored to specific steps in the assignment and structure refinement stages of analysis (see Chapter 26). Multidimensional NMR now plays a central part in the determination of the structures of large biomolecules (see Chapter 34), complementing and occasionally contradicting the results of X-ray diffraction, and providing unique insights into the internal motions and functional dynamics of proteins.

1.5 APPLICATIONS TO LIQUID CRYSTALS

Liquid crystalline samples are properly described as being liquids; the molecules in these phases move rapidly in all directions, but not randomly. The nonrandom motion leads to an incomplete averaging of the spin interactions within molecules, but essentially complete averaging between spins in different molecules. The Hamiltonian therefore contains terms for partially averaged anisotropic interactions such as the chemical shift anisotropy, the dipolar couplings, and, when spins $>1/2$ are present, the quadrupolar interaction. An NMR spectrum of a liquid crystalline sample thus has narrow lines, as in an isotropic liquid, but extra lines from the anisotropic interactions, as in solids. A liquid crystalline sample may, therefore, present different challenges to an NMR spectroscopist than those of isotropic liquid samples or of solids. The spectra that are observed depend crucially on whether an "aligned" sample can be created in the spectrometer. Alignment here refers to the mesophase directors, $\boldsymbol{n}_i$, which are unit vectors that at point i in the sample define the direction of average alignment for a group of neighboring molecules. The rapid motion of the molecules about the director leads to an averaging of a given magnetic interaction, A, such that only the component, A_{director}, along the director appears in the Hamiltonian. In an unconstrained sample, the director orientations are distributed isotropically and a broad powder spectrum is observed, similar to that for a polycrystalline solid. Methods for extracting the values of averaged NMR parameters from such a spectrum are similar to those used for solid samples and are not discussed here. However, it is possible to create a sample in which all the directors are aligned along a single direction, and now a spectrum with narrow lines is observed. Techniques for analyzing such spectra are similar to those used for normal liquids, but with some important differences. For nematic liquid crystalline samples, the uniform alignment occurs spontaneously on placing the sample in the magnetic field of the spectrometer. For other phases, the creation of an aligned sample can be more difficult, but may still be possible.[92]

Most of the nD spectra currently recorded on liquid crystalline samples are for proteins that have been partially oriented by dissolving in a weakly ordering medium. The orientational order of the protein molecules in these solutions is very small, such that the partially averaged dipolar couplings, usually referred to as *residual dipolar couplings* (RDCs), are similar in magnitude to the scalar spin–spin interactions and lead only to small changes in the spectra. Techniques appropriate for isotropic solutions are used for such samples.

The term *mesogen* is used to describe molecules whose presence in a liquid crystalline sample is essential for the stability of the phase. A liquid crystalline sample may contain only one mesogen, or several mesogens may be present. A distinguishing feature of mesogens is that their orientational order is large. To quantify this, consider two protons in such a molecule, separated by a distance r_{HH}. The partially averaged dipolar coupling, D_{ij}, between these two nuclei is given by

$$D_{ij} = -K_{ij}\left\langle \frac{(3\cos^2\theta_{ij} - 1)}{r_{ij}^3} \right\rangle \tag{1.8}$$

where

$$K_{ij} = \frac{\mu_0 \hbar \gamma_i \gamma_j}{16\pi^2} \tag{1.9}$$

The angular brackets in equation (1.8) denote an ensemble average, and θ_{ij} is the angle between the directions of r_{ij} and the applied magnetic field of the spectrometer. Note that the definition of the partially averaged dipolar coupling of equation (1.8) differs by a factor of 2 from that used commonly by structural biologists.

If the distance r_{ij} is fixed (apart from vibration), equation (1.8) can be rewritten as

$$D_{ij} = \frac{K_{ij}}{r_{ij}^3} S_{ij} \tag{1.10}$$

where the orientational order parameter S_{ij} for the direction r_{ij} is

$$S_{ij} = \frac{\langle 3\cos^2\theta_{ij} - 1\rangle}{2} \tag{1.11}$$

The order parameter must lie between $-1/2$ and 1, and for internuclear vectors in mesogenic molecules, it is typically in the range $|S_{ij}| = 0.1$–0.7; these values represent strong ordering. The proton spectra of mesogenic molecules are always second order, that is, the chemical shift differences are small compared with the total spin–spin couplings, $T_{ij} = J_{ij} + 2D_{ij}$. The dipolar couplings range in value over ~ -4000 to $+8000$ Hz. There are also many protons coupled to each other, so the spectrum is usually a broad unresolved band of resonances. ^{13}C spectra of mesogenic molecules also consist of broad, unresolved bands,

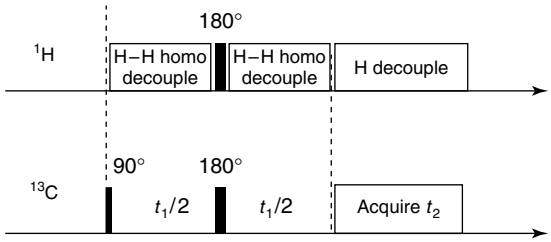

Figure 1.5. Pulse sequence for a separated local field experiment.

but can be dramatically simplified by removing all interactions with protons to give a spectrum consisting of a single peak for each group of equivalent ^{13}C nuclei, with chemical shifts:

$$\delta_i = \delta_i(\text{iso}) + \delta_i(\text{aniso}) \qquad (1.12)$$

where δ_i(iso) is the shift without orientational order and δ_i(aniso) is dependent on the order parameters $S_{\alpha\beta}$ for axes α and β fixed in the molecule.

Multidimensional experiments that are used specifically with liquid crystalline samples are designed either to assign the transitions in a well-resolved 1D spectrum, or to extract residual anisotropic interactions when a 1D spectrum is unresolved. An example of the latter type is the separated local field (SLF) 2D experiment, which was shown at an early stage in the development of 2D methods (see 1.2) to have the potential to dramatically improve the information that could be obtained on mesogenic molecules.[32] The basic pulse sequence is shown in Figure 1.5.

In the evolution period t_1, the protons are subjected to a multiple pulse sequence designed to eliminate dipolar coupling between the protons. This has the effect that the carbon magnetization evolves during t_1 under the influence of an effective Hamiltonian, $\hat{H}^0_{\text{eff}}$, where the superscript zero implies that it is the zeroth order in an average Hamiltonian expansion of the form:

$$\hat{H}^0_{\text{eff}} = k_{\text{CS}}\hat{H}^Z_{\text{H}} + k_{\text{CH}}\hat{H}^T_{\text{CH}} + k_{\text{HH}}\hat{H}^{\text{dipolar}}_{\text{HH}} + \hat{H}^J_{\text{HH}} + \hat{H}^Z_{\text{C}} \qquad (1.13)$$

The scaling factors, $k_{\text{CS}}, k_{\text{CH}}$ and k_{HH} depend in magnitude on the nature of the homodecoupling sequence used, which is intended to scale $\hat{H}^{\text{dipolar}}_{\text{HH}}$, representing the dipolar interactions between protons, to zero. Note that the scalar coupling term between protons, $\hat{H}^J_{\text{HH}}$, is unaffected by the multipulse sequence. The homodecoupling sequence applied to the protons changes the evolution of the carbon nuclei as a function of t_1 from being under the influence of a set of strongly coupled protons, to being effectively coupled only to a weakly coupled set. The SLF experiment follows ^{13}C magnetization in both t_1 and t_2 time intervals, and the resulting 2D spectrum has scaled total couplings, k_{CH} ($J_{\text{CH}} + 2D_{\text{CH}}$) in the F_1 domain, and the proton-decoupled ^{13}C spectrum in F_2. The scaling constant is dependent on the homonuclear decoupling sequence used, and can be determined by experiment. Each ^{13}C nucleus in the F_1 domain is split successively by each group of equivalent protons. This leads to increasingly crowded spectra as the number of protons increases. The experiment was improved in a fundamental way by using the pulse sequence of Figure 1.6. Now the proton magnetization is followed in t_1, while still detecting the ^{13}C magnetization in t_2. The resulting 2D spectrum, usually known as a *proton-encoded local field* (PELF), or *proton-detected local field* (PDLF), spectrum, again has scaled total couplings in F_1, but now the ^{13}C nuclei show a doublet splitting from each group of equivalent protons. This produces better resolution, particularly of distant protons (see Chapter 31).

The PDLF experiment gives the most useful, quantitative information for studying the structure,

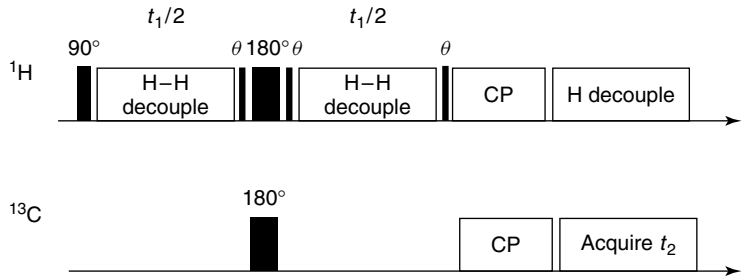

Figure 1.6. The ^{1}H–^{13}C 2D PDLF pulse sequence.

conformation, and orientational order of mesogens. It requires a spectrometer with the capability to decouple large $^{13}C-^{1}H$ interactions, which, in practice, means one designed to study solid samples; these are becoming increasingly widely available. Note, however, that the proton decoupling fields required are of the order of 50 kHz rather than the 100 kHz or more used for solid samples. Even though a relatively modest decoupling power is used, it is still necessary to take care not to raise the temperature of the sample during the experiment, typically by using decoupling only during acquisition, and by having a delay between pulse cycles of ~10 s.

Most NMR studies on mesogens, however, use ^{2}H NMR, and now the spectra are dominated by the partially averaged quadrupolar splittings, $\Delta\nu_i$, which, for mesogenic molecules, can be as large as 100 kHz. Each equivalent group of nuclei in the molecule gives a doublet centered on the ^{2}H chemical shift, and there may be smaller splittings on each doublet from dipolar coupling between nuclei within the equivalent group or to neighboring groups. A $^{2}H-^{2}H$ 2D COSY experiment can identify the doublets connected by the quadrupolar interaction, and may also reveal connections from dipolar coupling, even when the dipolar splittings are masked by large linewidths.[93] Early experiments required ^{2}H-enriched mesogens, and so had a limited number of applications. More recently, this experiment has been revived and improved for use on liquid crystalline samples produced by dissolving a synthetic polypeptide, such as poly-γ-benzyl-L-glutamate (PBLG), in an organic solvent such as chloroform. Such a solution forms a phase in which the local directors form a helical structure because of the chirality of the mesogenic molecules, the PBLG polymer units. When this phase is placed in a magnetic field, such as that of the NMR spectrometer, the helices unwind and an aligned nematic phase is produced, in which the chiral PBLG units impart a chirality to the phase. The interesting property of such a phase is that chiral solutes in this solvent give a different NMR spectrum for each enantiomer. The spectra differ because the dissolved enantiomers have different orientational order parameters, which leads to different anisotropic nuclear spin interactions such as the chemical shift anisotropy, the dipolar interaction, and for spins $>1/2$, the quadrupolar splittings. A ^{2}H spectrum of deuterated enantiomeric mixtures in a PBLG-solvent liquid crystalline solution consists of two overlapping spectra; 2D methods can be used to assign the lines to the separate optical isomers, but not to assign them to specific enantiomeric species[94] (see Chapter 29). The orientational order of solutes in the PBLG/solvent mixture is small ($S \sim 0.05$) and the residual quadrupolar splittings are typically in the range of -1000 to $+2000$ Hz, which means that spectra, including those in which decoupling is used, can be obtained on spectrometers designed for high-resolution studies of isotropic liquids.

Deuterium NMR of chiral solutes dissolved in a PBLG/solvent mixture is a very powerful method for distinguishing between enantiomers, particularly now that spectra can be obtained at the natural abundance level of deuterium (~0.015%).[95] Spectra from ^{13}C and ^{1}H are, however, useful for small chiral molecules, and several standard 2D experiments can be used to simplify their complex overlapping spectral patterns. Such experiments are usually designed to separate lines from different enantiomers so that the enantiomeric excess can be measured.

When investigating the structure of a molecule from a set of residual dipolar couplings it is desirable to measure as many couplings as possible between the magnetic nuclei in the molecule. Thus, for small hydrocarbons, it is relatively easy to obtain a well-resolved ^{1}H spectrum, which can be analyzed to provide all the interproton residual dipolar couplings, D_{ij}^{HH}, and, in a separate experiment, to record, less easily, a well-resolved and analyzable spectrum of the ^{13}C nuclei at natural abundance (~1%) to obtain a set, D_{ij}^{CH}, of $^{1}H-^{13}C$ couplings. Residual dipolar couplings can be very sensitive to the temperature of the sample, and the use of different experimental methods to determine the sets D_{ij}^{HH} and D_{ij}^{CH} may lead to their being measured at slightly different temperatures. This problem is eliminated by obtaining the set D_{ij}^{CE} by detecting and analyzing the weak satellite lines in the ^{1}H spectrum from molecules containing a single ^{13}C nucleus. Identifying which of the satellite lines belongs to which isotopomer can be a formidable task, made much easier by 2D experiments such as HSQC. For isotropic solutions, HSQC is often used simply as an assignment method, but here it is used to provide a separate ^{1}H spectrum for the proton(s) coupled to each different ^{13}C site.

As an example, consider the molecule $ClCH_2CH_2Br$, which in a liquid phase has rotational averaging about the C–C bond. The four protons form an AA′BB′ oriented spin system from which it is possible to extract four residual dipolar couplings between the protons, but these are insufficient in number to

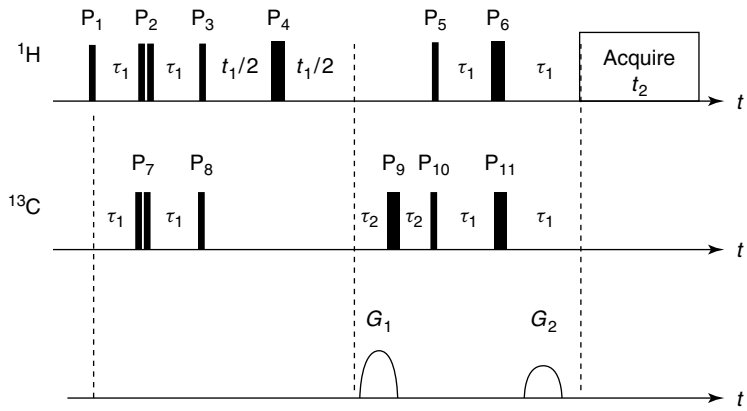

Figure 1.7. Pulse sequence to obtain HSQC spectra with ^{13}C shifts in F_1 and the ^{13}C-coupled proton spectrum in F_2. The delay τ_1 is adjusted to give the best intensity for the proton spectrum, while τ_2 is just long enough to include the gradient pulses G_1 and $G_2 = 1/2G_1$; quadrature detection in F_1 is achieved by N,P pathway selection, alternating the sign of G_1.

determine both the orientational order and the nature of the bond rotational potential, even when the bond lengths and angles are known or assumed. The two molecules $Cl^{13}CH_2CH_2Br$ and $ClCH_2{}^{13}CH_2Br$ give lines in the proton spectrum which, if they could be seen, would yield four residual couplings between protons and carbons. Unfortunately, these lines are difficult to detect in the presence of the strong lines from the abundant all-^{12}C molecules. The HSQC experiment reveals the satellite lines, as shown in Figure 1.8 for $ClCH_2CH_2Br$ dissolved in the liquid crystalline solvent ZLI 1132,[96] using the pulse sequence shown in Figure 1.7.

The version of the HSQC pulse sequence shown in figure 1.7 uses two INEPT modules to transfer magnetization between protons and carbons, and the efficiency of transfer depends on the value of τ_1. For isotropic samples, the optimum value of τ_1 depends on the magnitudes of the scalar couplings $^1J_{CH}$, which do not vary much between different molecules and are easily estimated. Liquid crystalline samples are very different. Now the efficiency depends on the values of the total spin–spin couplings, $^nT_{CH}$, which may be considerably larger than the scalar couplings and which also depend strongly on the orientational order of the molecules. Simulations of HSQC spectra for the case of $Cl^{13}CH_2CH_2Br$ and $ClCH_2{}^{13}CH_2Br$ have shown that there is a strong dependence of the line intensities in the HSQC experiment on τ_1, and it is essential to optimize this value experimentally using a 1D variant of the experiment.[96]

1.6 CONCLUDING REMARKS

No other spectroscopic technique approaches the versatility or sophistication of magnetic resonance. If NMR were unknown, and a thoughtful chemist set out to design an ideal form of spectroscopy, he or she might start out with a request that the parameters measured should reflect the most fundamental of chemical quantities, electron density, and report directly on the nature and location of chemical bonds. The timescale of the phenomenon studied should be readily accessible experimentally, and the range of parameter values such that large numbers of chemically distinct sites are resolvable in a spectrum.

Remarkably, even in its earliest incarnations NMR met all of these requirements. While one might occasionally wish that nature had been a little more generous with the magnetogyric ratio or the natural abundance of a favorite isotope, in almost every other respect, NMR is an ideal tool for the study of chemical structure. It would, however, have taken a very perceptive chemist indeed to ask also that the quantum-mechanical basis of the technique involve a bounded range of states, and make it experimentally easy to drive the spectroscopic response into nonlinearity: and yet it is the latter features of NMR that lie at the root of the great success of multidimensional NMR methods. This book sets out to explain and to illustrate the consequences that flow from the relative ease with which nuclear spin coherences can be created,

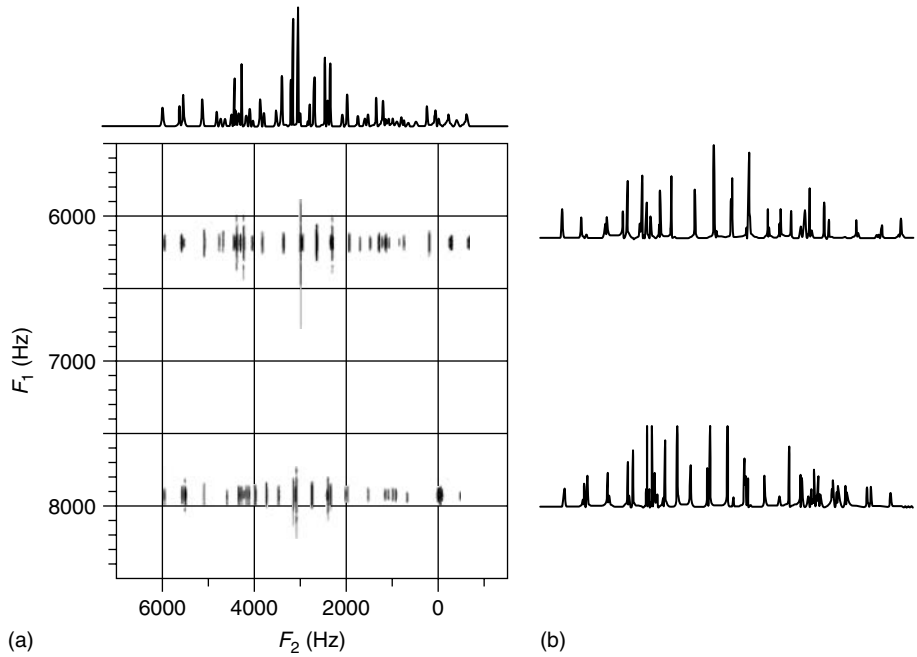

Figure 1.8. The 2D HSQC spectrum, for ^{1}H at 600 MHz and ^{13}C at 150 MHz (a), and the F_2 cross sections corresponding to the two ^{13}C shifts (b), for a sample of $ClCH_2CH_2Br$ dissolved in the liquid crystalline solvent ZLI 1132. (Reproduced, with permission, from Ref. 96.)

manipulated, and observed, and the profound implications that this has for many applications of NMR.

RELATED ARTICLES IN THE ENCYCLOPEDIA OF MAGNETIC RESONANCE

Chiral Discrimination Using Chiral Ordering Agents

Concentrated Solution Effects

Dipolar Field and Radiation Damping: Collective Effects in Liquid-state NMR

Echo-Planar Imaging

Field Gradients and Their Application

INEPT

Liquid Crystals: General Considerations

Phase Cycling

Projection–Reconstruction in MRI

REFERENCES

1. R. R. Ernst and W. A. Anderson, *Rev. Sci. Instrum.*, 1966, **37**, 93.
2. R. R. Ernst, *Chimia*, 1975, **29**, 179.
3. J. Jeener, Reminiscences about the early days of 2D NMR, in *Encyclopedia of Magnetic Resonance*, eds R. K. Harris and R. E. Wasylishen, John Wiley & Sons: Chichester. DOI: 10.1002/9780470034590.emrhp0087.
4. A. F. Mehlkopf, D. Korbee, T. A. Tiggelman, and R. Freeman, *J. Magn. Reson.*, 1984, **58**, 315.
5. R. R. Ernst, The success story of Fourier transformation in NMR, in *Encyclopedia of Magnetic Resonance*, eds R. K. Harris and R. E. Wasylishen, John Wiley & Sons: Chichester. DOI: 10.1002/9780470034590.emrhp0051.

6. J. S. Waugh, Alchemy of nuclear spins, in *Encyclopedia of Magnetic Resonance*, eds R. K. Harris and R. E. Wasylishen, John Wiley & Sons: Chichester. DOI: 10.1002/9780470034590.emrhp0191.
7. R. K. Hester, J. L. Ackerman, V. R. Cross, and J. S. Waugh, *Phys. Rev. Letters*, 1975, **34**, 993–995.
8. L. Müller, A. Kumar, and R. R. Ernst, *J. Chem. Phys.*, 1975, **63**, 5490.
9. M. Alla and E. Lippmaa, *Chem. Phys. Letters*, 1976, **37**, 260.
10. W. P. Aue, E. Bartholdi, and R. R. Ernst, *J. Chem. Phys.*, 1976, **64**, 2229.
11. W. P. Aue, J. Karhan, and R. R. Ernst, *J. Chem. Phys.*, 1976, **64**, 4226.
12. G. Bodenhausen, R. Freeman, and D. L. Turner, *J. Chem. Phys.*, 1976, **65**, 839.
13. G. Bodenhausen, R. Freeman, R. Niedermeyer, and D. L. Turner, *J. Magn. Reson.*, 1976, **24**, 291.
14. R. L. Vold and S. O. Chan, *J. Chem. Phys.*, 1970, **53**, 449.
15. R. Freeman and H. D. W. Hill, *J. Chem. Phys.*, 1971, **54**, 301.
16. G. Bodenhausen, R. Freeman, R. Niedermeyer, and D. L. Turner, *J. Magn. Reson.*, 1977, **26**, 133.
17. P. Bachmann, W. P. Aue, L. Müller, and R. R. Ernst, *J. Magn. Reson*, 1977, **28**, 29.
18. G. Bodenhausen, R. Freeman, and D. L. Turner, *J. Magn. Reson.*, 1977, **27**, 511.
19. K. Nagayama, K. Wüthrich, P. Bachmann, and R. R. Ernst, *Naturwissenschaften*, 1977, **64**, 581.
20. K. Nagayama, The first protein two-dimensional (2D) NMR, in *Encyclopedia of Magnetic Resonance*, eds R. K. Harris and R. E. Wasylishen, John Wiley & Sons: Chichester. DOI: 10.1002/9780470034590.emrhp0130.
21. K. Nagayama, K. Wüthrich, P. Bachmann, and R. R. Ernst, *Biochem. Biophys. Res. Commun.*, 1977, **78**, 99.
22. K. Wüthrich, in *Encyclopedia of Magnetic Resonance*, eds R. K. Harris and R. E. Wasylishen, John Wiley & Sons: Chichester. DOI: 10.1002/9780470034590.emrhp0201.
23. K. Wüthrich, *NMR of Proteins and Nucleic Acids*, Wiley: New York, 1986.
24. A. A. Maudsley and R. R. Ernst, *Chem. Phys. Lett.*, 1977, **50**, 368.
25. A. A. Maudsley, L. Müller, and R. R. Ernst, *J. Magn. Reson.*, 1977, **28**, 463.
26. R. Freeman and G. A. Morris, *J. Chem. Soc. Chem. Commun.*, 1978, 684.
27. A. Bax and M. F. Summers, *J. Am. Chem. Soc.*, 1986, **108**, 2093.
28. G. Bodenhausen and D. J. Ruben, *Chem. Phys. Lett.*, 1980, **69**, 185.
29. A. Bax, R. H. Griffey, and B. L. Hawkins, *J. Am. Chem. Soc.*, 1983, **105**, 7188.
30. W. P. Aue, P. Bachmann, A. Wokaun, and R. R. Ernst, *J. Magn. Reson.*, 1978, **29**, 523.
31. R. Freeman, G. A. Morris, and D. L. Turner, *J. Magn. Reson.*, 1977, **26**, 373.
32. G. Bodenhausen, R. Freeman, G. A. Morris, and D. L. Turner, *J. Magn. Reson.*, 1977, **28**, 17.
33. (a) A. Kumar, *J. Magn. Reson.*, 1978, **30**, 227; (b) *J. Magn. Reson.*, 1980, **40**, 413.
34. G. Bodenhausen, R. Freeman, G. A. Morris, and D. L. Turner, *J. Magn. Reson.*, 1978, **31**, 75.
35. K. Nagayama, P. Bachmann, K. Wüthrich, and R. R. Ernst, *J. Magn. Reson.*, 1978, **31**, 133.
36. P. H. Bolton and G. Bodenhausen, *J. Am. Chem. Soc.*, 1979, **101**, 1080.
37. A. Höhener, L. Müller, and R. R. Ernst, *Mol. Phys.*, 1979, **38**, 909.
38. B. H. Meier and R. R. Ernst, *J. Am. Chem. Soc.*, 1979, **101**, 6441.
39. J. Jeener, B. H. Meier, P. Bachmann, and R. R. Ernst, *J. Chem. Phys.*, 1979, **71**, 4546.
40. D. Neuhaus and M. P. Williamson, *The Nuclear Overhauser Effect in Structural and Conformational Analysis*, 2nd edn., Wiley-VCH: New York, 2000.
41. R. Freeman and G. A. Morris, *Bull. Magn. Reson.*, 1979, **1**, 5.
42. A. Bax, *Two-Dimensional Nuclear Magnetic Resonance in Liquids*, Delft University Press/D Reidel: Dordrecht, 1982.
43. G. Eich, G. Bodenhausen, and R. R. Ernst, *J. Am. Chem. Soc.*, 1982, **104**, 3731.
44. P. H. Bolton and G. Bodenhausen, *Chem. Phys. Lett.*, 1982, **89**, 139.
45. A. Bax, R. Freeman, and S. P. Kempsell, *J. Am. Chem. Soc.*, 1980, **102**, 4849.
46. A. Bax, R. Freeman, T. A. Frenkiel, and M. H. Levitt, *J. Magn. Reson.*, 1981, **43**, 478.
47. U. Piantini, O. W. Sørensen, and R. R. Ernst, *J. Am. Chem. Soc.*, 1982, **104**, 6800.

48. L. Braunschweiler and R. R. Ernst, *J. Magn. Reson.*, 1983, **53**, 521.
49. A. A. Bothner-By, R. L. Stephens, J. M. Lee, C. D. Warren, and R. W. Jeanloz, *J. Am. Chem. Soc.*, 1984, **106**, 811.
50. D. J. States, R. A. Haberkorn, and D. J. Ruben, *J. Magn. Reson.*, 1982, **48**, 286.
51. D. Marion and K. Wüthrich, *Biochem. Biophys. Res. Commun.*, 1983, **113**, 967.
52. J. Keeler and D. Neuhaus, *J. Magn. Reson.*, 1985, **63**, 454.
53. A. L. Davis, E. D. Laue, J. Keeler, D. Moskau, and J. Lohman, *J. Magn. Reson.*, 1991, **94**, 637.
54. C. Griesinger, O. W. Sørensen, and R. R. Ernst, *J. Am. Chem. Soc.*, 1985, **107**, 6394.
55. R. E. Hurd, *J. Magn. Reson.*, 1990, **87**, 422.
56. R. E. Hurd, Field Gradients and Their Application, in *Encyclopedia of Magnetic Resonance*, eds R. K. Harris and R. E. Wasylishen, John Wiley & Sons: Chichester. DOI: 10.1002/9780470034590.emrstm0164.
57. G. Bodenhausen, H. Kogler, and R. R. Ernst, *J. Magn. Reson.*, 1984, **58**, 370.
58. D. L. Turner, Phase Cycling, in *Encyclopedia of Magnetic Resonance*, eds R. K. Harris and R. E. Wasylishen, John Wiley & Sons: Chichester. DOI: 10.1002/9780470034590.emrstm0389.
59. G. W. Vuister and R. Boelens, *J. Magn. Reson.*, 1987, **73**, 328.
60. L. E. Kay, G. M. Clore, A. Bax, and A. M. Gronenborn, *Science*, 1990, **249**, 411.
61. A. Bax and S. Grzesiek, *Acc. Chem. Res.*, 1993, **26**, 131.
62. K. F. Morris and C. S. Johnson Jr., *J. Am. Chem. Soc.*, 1992, **114**, 3139.
63. C. S. Johnson Jr., *Prog. Nucl. Magn. Reson. Spectrosc.*, 1999, **34**, 203.
64. P. Stilbs, *Anal. Chem.*, 1981, **53**, 2135.
65. H. Barkhuijsen, R. de Beer, W. M. M. J. Bovée, and D. van Ormondt, *J. Magn. Reson.*, 1985, **61**, 465.
66. H. Gesmar, J. J. Led, and F. Abildgaard, *Prog. Nucl. Magn. Reson. Spectrosc.*, 1990, **22**, 255.
67. J. W. Pang, T. Dieckmann, J. Feigon, and D. Neuhauser, *J. Chem. Phys.*, 1998, **108**, 8360.
68. V. A. Mandelshtam, H. S. Taylor, and A. J. Shaka, *J. Magn. Reson.*, 1998, **133**, 304.
69. D. M. Korzhnev, I. Ibraghimov, M. Billeter, and V. Y. Orekhov, *J. Biomol. NMR*, 2001, **21**, 263.
70. Ē. Kupče and R. Freeman, *J. Magn. Reson.*, 2003, **162**, 158–165.
71. S. Kim and T. Szyperski, *J. Am. Chem. Soc.*, 2003, **125**, 1385–1393.
72. R. Brüschweiler and F. Zhang, *J. Chem. Phys.*, 2004, **120**, 5253–5260.
73. O. Cloarec, M. E. Dumas, A. Craig, R. H. Barton, J. Trygg, J. Hudson, C. Blancher, D. Gauguier, J. C. Lindon, E. Holmes, and J. Nicholson, *Anal. Chem.*, 2005, **77**, 1282–1289.
74. G. H. Glover and J. M. Pauly, Projection-reconstruction in MRI, in *Encyclopedia of Magnetic Resonance*, eds R. K. Harris and R. E. Wasylishen, John Wiley & Sons: Chichester. DOI: 10.1002/9780470034590.emrstm0417.
75. Ē. Kupče and R. Freeman, *J. Am. Chem. Soc.*, 2004, **126**, 6429–6440.
76. P. Mansfield, Echo-planar imaging, in *Encyclopedia of Magnetic Resonance*, eds R. K. Harris and R. E. Wasylishen, John Wiley & Sons: Chichester. DOI: 10.1002/9780470034590.emrstm0145.
77. L. Frydman, T. Scherf, and A. Lupulescu, *Proc. Natl. Acad. Sci. U.S.A.*, 2002, **99**, 15858.
78. R. Freeman, S. P. Kempsell, and M. H. Levitt, *J. Magn. Reson.*, 1977, **34**, 663.
79. M. H. Levitt, G. Bodenhausen, and R. R. Ernst, *J. Magn. Reson.*, 1983, **53**, 443.
80. A. J. Pell and J. Keeler, *J. Magn. Reson.*, 2007, **189**, 293.
81. Ē. Kupče and R. Freeman, *Magn. Reson. Chem.*, 2007, **45**, 711.
82. Ē. Kupče and R. Freeman, *J. Magn. Reson.*, 2008, **191**, 164.
83. K. Zangger and H. Sterk, *J. Magn. Reson.*, 1997, **124**, 486.
84. R. Freeman and H. D. W. Hill, *J. Magn. Reson.*, 1971, **4**, 366.
85. A. E. Derome and M. P. Williamson, *J. Magn. Reson.*, 1990, **88**, 177.
86. M. H. Levitt, *Concepts Magn. Reson.*, 1996, **82**, 77.
87. J. Jeener, Concentrated solution effects, dipolar field and radiation damping: collective effects in liquid-state NMR, in *Encyclopedia of Magnetic*

Resonance, eds R. K. Harris and R. E. Wasylishen, John Wiley & Sons: Chichester. DOI: 10.1002/9780470034590.emrstm0124.

88. P. J. Bowyer, A. G. Swanson, and G. A. Morris, *J. Magn. Reson.*, 1999, **140**, 513.
89. L. Bollans, D. O'Farrell, J. Bacsa, J. A. Iggo, G. A. Morris, and A. V. Stachulski, *Org. Biomol. Chem.*, 2009, **7**, 4531.
90. J. K. M. Sanders and B. K. Hunter, *Modern NMR Spectroscopy*, 2nd edn., Oxford University Press: Oxford, 1993.
91. R. K. Harris, R. E. Wasylishen, and M. J. Duer, *A Handbook of NMR Crystallography*, John Wiley & Sons: Chichester, 2009.
92. J. W. Emsley, Liquid crystals: general considerations, in *Encyclopedia of Magnetic Resonance*, eds R. K. Harris and R. E. Wasylishen, John Wiley & Sons: Chichester. DOI: 10.1002/9780470034590.emrstm0270.
93. J. W. Emsley and D. L. Turner, *Chem. Phys. Lett.*, 1981, **82**, 447.
94. J. Courtieu, P. Lesot, A. Meddour, D. Merlet, and C. Aroulanda, Chiral discrimination using chiral ordering agents, in *Encyclopedia of Magnetic Resonance*, eds R. K. Harris and R. E. Wasylishen, John Wiley & Sons: Chichester. DOI: 10.1002/9780470034590.emrstm0078.
95. J. Courtieu and P. Lesot, *Prog. Nucl. Magn. Reson. Spectrosc.*, 2009, **55**, 128.
96. J. W. Emsley, D. Merlet, K. J. Smith, and N. Suryaprakash, *J. Magn. Reson.*, 2002, **154**, 303.